Christian Doppler Forschungsgesellschaft

Graz University of Technology

Master Thesis

RSS-based Localization of Smart Labels

conducted at the
CD Laboratory for Location-aware Electronic Systems
Graz University of Technology, Austria

in co-operation with
SES imagotag GmbH
Graz, Austria

by
Franz Lampel BSc, 1230721

Supervisor:
Dipl.-Ing. Stefan Grebien BSc

Assessor/Supervisor:
Assoc.Prof. Dipl.-Ing. Dr. Klaus Witrisal

Graz, April 18, 2018

Abstract

Electronic Shelf Labels (ESL) are deployed in retail stores in order to display information such as price, origin, etc. to the customer. Location awareness of such ESLs (and thus of the products) gives rise to various applications. For customers, for instance geo-localization of the shopping list can be realized; for shop operators, the sales floor management can be optimized. ESLs are highly constrained in terms of price and energy consumption in order to achieve a high density of deployment and a long battery life time. This is of fundamental importance for a dedicated localization technique that can be applied for this purpose. ESLs use wireless communication technologies to update the displayed information. Radio-based localization techniques could thus offer a possibility to determine their location. The Received Signal Strength (RSS) is a measure which reflects the instantaneous power at the receiver and therefore provides location information. The advantage of the RSS is that it can be determined by low cost transceiver chips and so it can be utilized by localization algorithms without any hardware modifications of the ESLs. On the other hand, RSS shows low accuracy and robustness in presence of multipath propagation, which dominates the wireless channel in indoor scenarios. This circumstance is addressed by a measurement campaign with the aim to characterize the wireless channel between ESLs for a typical shop layout. Different link conditions such as Line- of-Sight (LOS) and Non-Line-of-Sight (NLOS) were investigated. Based on the channel characterization, a localization strategy is proposed in order to move towards location awareness of ESLs, making them even smarter labels.

Kurzfassung

Electronic Shelf Labels (ESL) sind elektronische Kennzeichnungen, welche in Kaufhäusern eingesetzt werden und Informationen zu Produkten wie z. B. Preis, Ursprung, etc. anzeigen. Ortssensitivität von solchen ESLs, und damit die Ortbarkeit der Produkte, ermöglicht neue Anwendungen für Kunden, wie z. B. die Geolokalisierung der Einkaufsliste, und auch für die Betreiber von Geschäften welchen sie bei der Verwaltung ihrer Geschäftsflächen hilft. ESLs sind aufgrund ihrer Vielzahl und Batteriekapazität in ihrem Preis und Energieverbrauch stark beschränkt. Diese Beschränkung ist bei der Entwicklung einer speziellen Lokalisierungstechnik von großer Wichtigkeit. ESLs nützen drahtlose Übertragungstechnologien, um die angezeigte Information zu aktualisieren, und es liegt nahe, diese Technologie auch für die Lokalisierung zu nützen. Die empfangene Signalstärke ist eine Messgröße, welche Ortsinformation bietet. Sie reflektiert die momentane empfangene Leistung, welche wiederum von der Position der ESLs abhängt. Der Vorteil dieser Messgröße ist, dass sie selbst von billigen Empfängerchips bereitgestellt wird und dadurch von Lokalisierungsalgorithmen ausgenutzt werden kann, ohne die Hardware zu verändern. Der Nachteil der empfangenen Signalstärke als Messparameter ist die Ungenauigkeit, die aufgrund von Mehrwegeausbreitung des Signals entsteht. Dieser Umstand wurde in einer Messkampagne untersucht, welche einen Anwendungsfall eines ESLs nachbildet. Unterschiedliche Verbindungsbedingungen zwischen Sender und Empfänger wie z. B. Sichtverbindung und geblockte Sichtverbindung wurden berücksichtigt. Basierend auf den Beobachtungen wird eine Lokalisierungstechnik vorgeschlagen, um einen Schritt in Richtung Ortssensitivität von ESLs zu machen und damit die Labels noch schlauer zu machen.

Statutory Declaration

I declare that I have authored this thesis independently, that I have not used other than the declared sources/resources, and that I have explicitly marked all material which has been quoted either literally or by content from the used sources.

date	(signature)

Contents

1 Introduction **7**
1.1 Motivation . . . 7
1.2 Indoor Localization . . . 7
1.2.1 Time of Arrival . . . 8
1.2.2 Time Difference of Arrival . . . 8
1.2.3 Angle of Arrival . . . 8
1.2.4 Ultra Wide Band . . . 8
1.2.5 RSS-based Localization . . . 8
1.3 Hypothesis . . . 9
1.4 Outline . . . 10

2 Measurement Campaign **11**
2.1 Location . . . 11
2.1.1 Link Conditions . . . 12
2.2 Measurement Campaign - Channel Sounder . . . 13
2.2.1 Measurement Setup . . . 13
2.2.2 Link conditions . . . 17
2.3 Measurement Campaign - Electronic Shelf Label . . . 19
2.3.1 Measurement Setup . . . 19

3 Channel Characterization **21**
3.1 Channel Models in Literature . . . 21
3.1.1 Narrowband Model . . . 21
3.1.2 Wideband Models . . . 23
3.2 Evaluation of the measurements . . . 25
3.2.1 Narrowband Results . . . 25
3.2.2 Amplitude Distribution . . . 29
3.3 Wideband results . . . 30
3.3.1 Power Delay Profile . . . 31
3.4 Measurements with Electronic Shelf Labels . . . 37
3.5 Proposed channel model . . . 42
3.5.1 Validation of the Model . . . 44

4 Localization Algorithm **47**
4.1 Shelf Detection . . . 48
4.1.1 Evaluation . . . 49

5 Conclusion and Outlook **52**
5.1 Conclusion . . . 52
5.2 Outlook . . . 52

A ESL **53**
A.1 ESL Channels . . . 53
A.2 ESL Datasheet . . . 54

B Measurement Campaign - Channel Sounder **55**
B.1 Standard Scenarios . . . 55
B.1.1 NLOS, facing . . . 56
B.1.2 NLOS, aligned . . . 56
B.1.3 LOS 1 . . . 56

B.1.4 LOS 2 . . . 57
B.1.5 Rx Groups . . . 57
B.2 Special Scenarios . . . 57
B.2.1 Same Shelf . . . 57
B.2.2 LOS, dense spacing . . . 58
B.2.3 Groups on same shelf . . . 59

C Measurement Campaign - Electronic Shelf Label **61**
C.1 ESL Position . . . 61
C.2 RSSI Measurement . . . 62

1 Introduction

1.1 Motivation

Robust and accurate indoor localization has gained a lot of attention with respect to research in the past decades. With the emergence of the Internet of Things (IoT), location awarness is considered a key enabler for many applications like assisted living, logistics and production [1]. This research work focuses on the localization of Electronic Shelf Labels (ESL) which are mainly deployed in retail shops. These ESLs are attached to shelfs/racks next to a product and display important information for the customers such as price, origin, etc. Since ESLs use wireless communication technologies to update the displayed information, potentially by means of radio-based localization techniques. This location awareness make ESLs to *smart labels* since it opens way for the development of a wide range of customer centered applications. Instances of such applications are: geo-localization of the products of the shopping list, planning and optimization of the shopping route around the store, and influences the efficiency of floor management systems. Products tagged with location aware ESLs enable the floor management systems to update the floor plans according to their respective locations automatically. The usage of ESLs is not only restricted to the retail shops but they could also be used in production workshops for part/device labeling.

Figure 1.1: Application of ESLs [2], ©SES imagotag

1.2 Indoor Localization

Outdoor localization systems based on Global Navigation Satellite Systems (GNSS), such as GPS, are usually not available for indoor localization, thus making way for other technologies to carry out the desired tasks [3]. Different methods of indoor localizations are studied in the literature [4].

1.2.1 Time of Arrival

Time of Arrival (ToA) methods estimate measures the propagation time of a signal transmitted by anchor nodes with known position to a target node with unknown position. Based on the propagation time can the distance between the anchor nodes and the target node be estimated. If different distance estimates from anchors are available, multilateration can be used to estimate the position of the target node. Since this method is based on the absolute arrival time of the signal, all nodes have to be synchronized. Another requirement is that the positions of the source nodes must be known. Based on the dimensionality of the localization problem, at least three source nodes are needed for a 2D problem in order to obtain a unique solution. Whereas, for a 3-D localization problem, at least four source nodes are required.

1.2.2 Time Difference of Arrival

For the ToA approach, a tight synchronization between all nodes is needed. Time Difference of Arrival (TDoA) tries to overcome the synchronization requirement of all nodes in the ToA approach. In this approach just the anchor nodes need to be synchronized. The position can be estimated by the differences of the propagation time between transmitted signals from the anchor nodes.

1.2.3 Angle of Arrival

Angle of Arrival (AoA) also known as the Direction of Arrival (DoA) approach estimates the position of the target node by means of the arrival direction. This is carried out as the signal is received at the target node. This approach drops the requirement of synchronizing the nodes. However, at the same time another requirement arises, since the AoA of a signal has to be estimated. For instance, this can be done with the help of antenna arrays. Another advantage of the AoA approach is that it reduces the number of source nodes. In ToA the position is estimated based on intersections of circles. The position in AoA methods is estimated on the intersection of lines and therefore just two source nodes are needed for 2-D problems. Whereas, for the 3-D problem three source nodes are required. It is similar to the ToA and TDoA localization methods in the sense that it also requires the position of the anchor nodes to be known.

1.2.4 Ultra Wide Band

Ultra Wideband (UWB) signals [5] have been exploited to determine the position of the subject under study in particular in indoor environments. UWB signals occupy a bandwidth in the order of hundreds of MHz and thus are localized in time with a high accuracy. This in turn leads to resolvable specular multipath which can be exploited for localization by utilizing knowledge about the floor plan.

1.2.5 RSS-based Localization

The drawback for ESLs of the localization techniques discussed so far is that they need dedicated hardware. An alternative to the discussed approaches is by localization based on the Received Signal Strength (RSS). The RSS is a parameter which reflects the instantaneous signal power and is provided by many different low-cost technologies such as Wi-Fi, bluetooth, etc. This is also valid for ESLs, since the used transceiver chip provides a Received Signal Strengh Indicator (RSSI) for the received signal and can therefore be used without changing the hardware. The requirements of low complexity and low cost localization make RSS-based localization an

interesting approach. Therefore, RSS-based localization has become of interest for the research community and different approaches are investigated. The major drawback of RSS as a position indicator is its low accuracy due to multipath and non line of sight propagation (NLOS). This is especially valid for shops since they represent a large scattering environment because of the vast amount of objects which are present in a sales floor. Another source of unstability of RSS values are people who are present during opening hours [6]. In general, there are three different approaches which dominate the RSS-based localization, namely: localization based on a radio propagation model, fingerprinting and machine learning techniques such as Gaussian process regression [4, 7].

Model-based RSS Localization

Localization based on a radio propagation model takes advantage of the distance information which is contained inherently in the RSS-value due to a path loss model. The position of the receiver can be calculated based on the distance estimation to different transmitters with known position. The main disadvantage of this approach is that other parameters than the distance have to be estimated as well. Different algorithms and assumptions about the radio propagation model have been applied to overcome ambiguities in the RSS-distance relationship [8–10].

Fingerprinting-based RSS Localization

Another approach which is investigated and deployed is so called fingerprinting. In fingerprinting, RSS-values from different Access Points (AP) are collected at a dense mesh of points and stored in a database during a training/offline phase. In the localization/online phase, RSS-values are collected by a user device and compared with the values stored in the database [11]. For decision making regarding the position of a device, different approaches are applied such as k-nearest-neighbours (knn) [12], etc. Fingerprinting is advantageous in comparison to the multilateration approach in the sense that it does not require a signal model and also does not need any complex parameter estimation. The main drawback of fingerprinting is that the generation of the database is labour intensive and has to be updated whenever a change in the environment occurs.

Gaussian Process Regression for RSS Indoor Localization

An attractive method to overcome these problems are Gaussian processes. In this context, Gaussian process is a machine learning technique for regression tasks [7]. Gaussian process typically utilizes a generic signal model with parameters that are being learned from data. Like fingerprinting, Gaussian process has to be trained and therefore the accuracy depends on the spacing of the training points. On the other hand, it takes advantage of the spatial correlation of the RSS values and uses this correlation information to predict the RSS at an location where no measurment has been reported before. The result of a Gaussian Process is a posterior distribution over functions and can therefore be used to predict the position of a device by a maximum likelihood approach. The combination of different approaches have also been studied to increase the accuracy of the estimated position [13, 14].

1.3 Hypothesis

RSS based localization techniques studied in literature show position errors in the order of meters. Localization of ESLs requires higher accuracy since a position error of some meters could map an estimated position onto a wrong shelf or even corridor. The objective of this thesis

is therefore to evaluate the possibility of detecting the correct shelf and position by exploiting RSSI measurements in-between ESLs. It is assumed that the extremely dense deployment of ESLs in retail-store environments can be utilized to achieve position errors in the sub-meter range.

1.4 Outline

The remaining part of the thesis is structured as follows: In Chapter 2 a channel measurement campaign is described. In Chapter 3 existing channel models are described and the measured channel impulse responses (CIR) are evaluated. Based on the results from the evaluation of the measured CIRs, a channel model is introduced. The proposed channel model is tested against the measured CIRs in terms of their statistical behavior. In Chapter 4 a localization algorithm is introduced and tested against real data. Finally, Chapter 5 presents an outlook on future work.

2 Measurement Campaign

The indoor wireless channel is quite dynamic in the sense that it depends on the multipath propagation and therefore on the propagation environment. The layout and the interacting objects (IO) in the propagation environments play a vital role. This issue is usually addressed by doing channel measurements. These channel measurements focus on different propagation environments such as offices or industrial environments as well as different frequency bands. Another important influence is given by the vast amount of shelves which form corridors. These corridors are variable in height and depend in our case on the type of shop. For instance, grocery stores are usually equipped with shelves which have typical heights in the order of 2 m while in multimedia stores shelves with lower height can be found. Another factor which is of paramount importance is the antenna directivity. To conclude, it is not possible to give a general channel model for a link between ESLs. This measurement campaign aims to evaluate the CIR for a generic and simple setup. Further measurements in real shops could give more insight about propagation mechanisms found in shops.
Two measurement campaigns were carried out. The first one was done with a channel sounder which offers the possibility to determine the wideband characteristics as well as the narrowband characteristics of the channel. The channel sounding via a channel sounder offers the possibility to focus on the channel characteristics independent of hardware impairments given for low cost ESLs. Regular ESLs were used for the second measurement campaign. The focus of this measurement campaign was to verify narrowband results obtained from the first measurement campaign. Moreover, it gives inside with respect to the stability and reciprocity in static scenarios.

2.1 Location

The measurement campaigns were carried out in the demo room of the Signal Processing and Speech Communication Laboratory which is located on the third floor of the study center at Inffeldgasse 10. The roomsize is about 45 m^2 and contains desks, chairs, windows and a whiteboard. The layout of the measurement campaign is illustrated in Figures 2.1 and 2.2. Corridors, which are formed by shelves, are usually found in shops. This fact is reproduced by the appropriate arrangment of eight shelves. The width of the corridor was 1.2 m which, according to sales floor regulation, is the smallest possible width of a corridor [15]. In real application scenarios, the shelf content varies significantly depending on the retail sector. No content was placed on the shelves within this initial measurement campaign. In orderer to block the direct link between the corridors was a metal grid placed between the pair of shelves S3/S6 and S4/S5. Further measurements could be used to characterize the influence of the shelf content on the wireless channel.

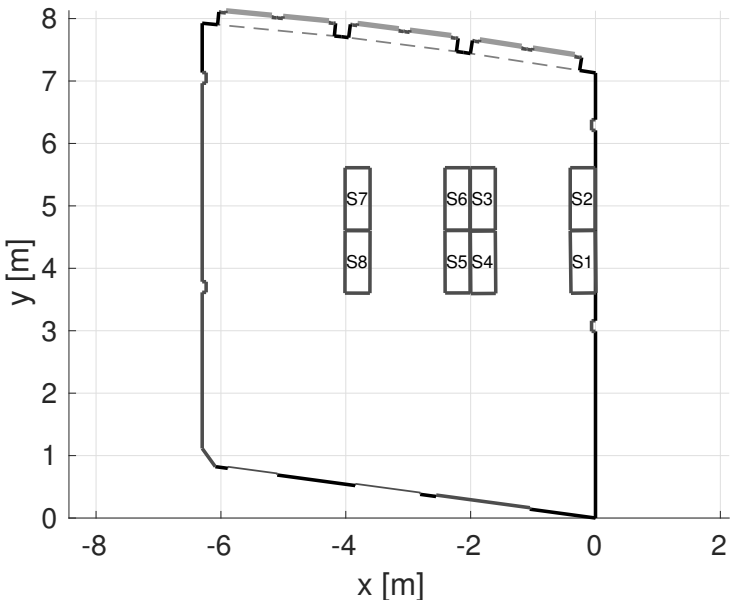

Figure 2.1: Layout of the demo room

Figure 2.2: Setup of the shelves

2.1.1 Link Conditions

The link condition between two ESLs is mainly governed by two facts, namely the LOS condition and the directivity. Therefore, five different link conditions between ESLs exist. These five link conditions can be divided into two main groups according to the LOS condition. The first group consists of links were the Line of Sight (LOS) link is not obstructed. This group can be subdivided into two links of pairs of ESLs on the same shelf and pairs of ESLs placed on opposite shelves. Such links can be found in scenarios were ESLs are placed in the same corridor. Throughout this thesis, these two link conditions will be referred to as *LOS, same shelf* and *LOS, facing*. The link conditions in the second main group share the feature that the LOS link is blocked by a shelf. The three link condition in this group can be described as follows: a *NLOS, facing* link is given for ESLs where the displays point to each other. This link is found for pairs of ESLs placed on the shelf pairs S7/S8 and S1/S2. The second link condition of the *NLOS* group is referred to as *NLOS, aligned* and is given for links where the azimuth orientation

of a pair of ESLs is aligned. An instance of such an link condition is given for links between ESLs placed on shelf S7/S8 and S3/S4. The last link condition is referred to *NLOS, back to back* and can be observed in the given layout for links between ESLs places on shelf S3/S4 and S5/S6. Table 2.1 provides an overview of the link conditions and if they were evaluated in the two measurement campaigns.

Link Condition		Measurement Campaign	
		Channel Sounder	ESL
LOS	same shelf	✓	✓
	facing	✓	✓
NLOS	aligned	✓	✓
	facing	✓	✓
	back to back	-	✓

Table 2.1: Link condition investigated in the measurement campaigns

2.2 Measurement Campaign - Channel Sounder

2.2.1 Measurement Setup

The channel sounding was done with the Ultra Wideband M-Sequence Device from ILMsens. A total number of nine ESLs was available for the measurement campaign. The measurement setup is depicted in Figure 2.3. Since the channel sounder offers one transmitter and two receivers, two switching devices were used to utilize all nine ESLs consecutively in each scenario. The channel sounder and the two switches were remote controlled by a PC. A detailed description of the used equipment can be found in Appendix B

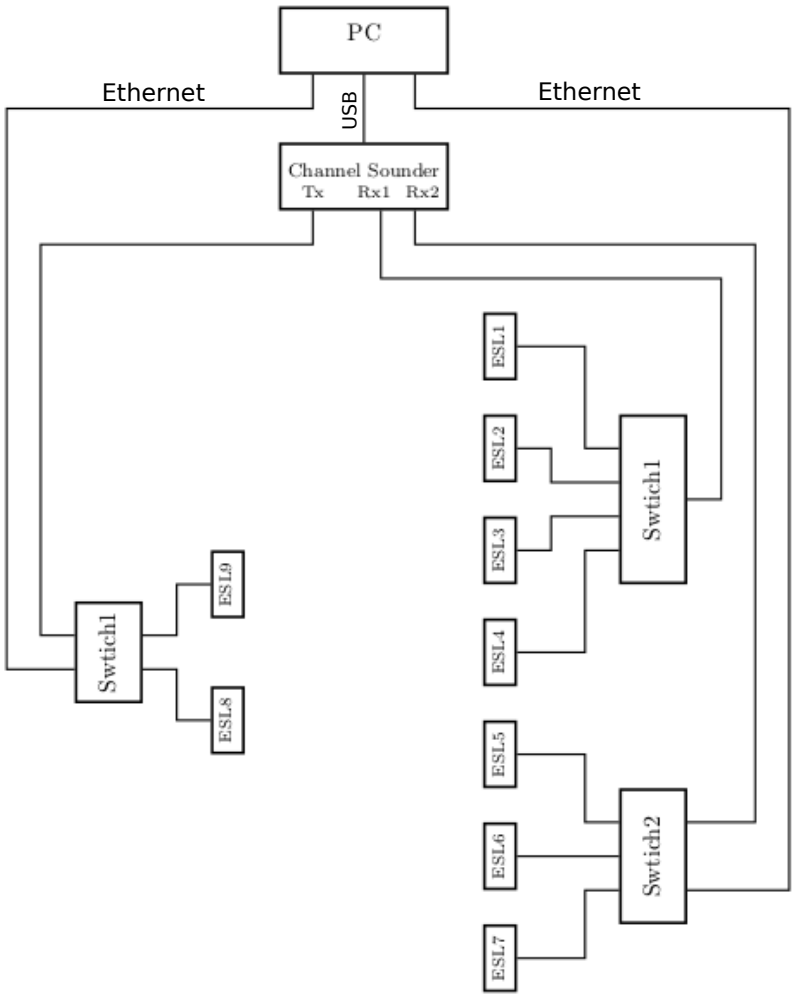

Figure 2.3: Block diagram of the setup

Channel Sounder

The used channel sounder is a correlative channel sounding device, utilizing a Maximum-Length Sequence (M-Sequence) which is a binary pseudo random sequence. The length of the M-sequence limits the dynamic range of the channel sounder. The used device has an M-sequence of length 2^{12} and the dynamic range DR is given therefore as

$$DR = 20 \cdot log_{10}\left(2^{12} - 1\right) = 72.24 \quad \text{dB}. \tag{2.1}$$

A detailed description of channel sounding techniques can be found in [16] and [17] while in [18] the used device and the calibration is described. In the baseband operation, the channel sounder utilizes the band ranging from 0.1 GHz to 3.2 GHz. The sampling rate is 6.95 GHz while the length of the measured CIRs is fixed to 4095 samples according to the length of the M-sequence. Synchronous averaging of 1024 CIRs was performed in order to increase the resulting SNR. The averaging requires a stationary channel for all measurements which can be assumed to be true since no moving objects where present during the measurement and the operators were not interacting with the measurement environment. The channel sounder was calibrated before the measurements were carried out. The calibration includes all cables and the switching devices up to the connector at the antenna in order to compensate for system loss and cross-talk within

the measurement system setup. The measured CIRs were corrected during post processing of the data.

Electronic Shelf Label

The objective of the measurement campaign was to obtain the CIRs between pairs of ESLs. Therefore, regular ESLs were used. The ESLs were modified for the purpose of the measurement campaign. The radiation pattern of the antenna was considered as part of the CIR. Therefore, a coaxiale cable with an SMA-connector was connected to the antenna of the ESL. The additional delay, introduced by the cables, is neglected in the overall meausrement since ToA localization principles are not of interest. This modification made it possible to carry out measurements directly with the channel sounder. The maximal useable bandwidth is determined by the antenna bandwidth of an ESL. The antenna bandwidth is defined as the frequency for which the S_{11} parameter (or reflection coefficient) is less than -6 dB [19]. Good matching of the antenna is obtained for S_{11} values below -10 dB. The S_{11} parameters of the nine used ESLs are depicted in Figure 2.4. It can be seen that the S_{11} parameter drops below -6dB for a bandwidth in the range from about 2.3 to 2.5 GHz. A quite large variation of the S_{11} parameter between the single ESLs can be seen. The bandwidth limits the spatial resolution of the multipath components of the measured CIRs. However, the aim of the measurement campaign is not to identify strong specular components since they are different in each indoor environment.

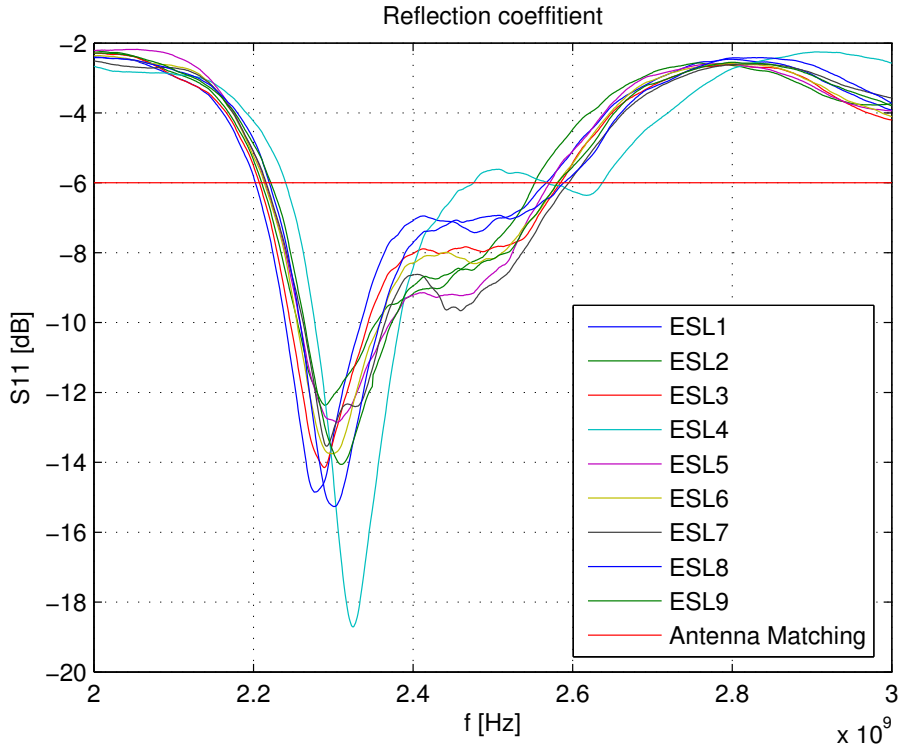

In Figure 2.4

Figure 2.4: S_{11} parameter of the nine used ESLs

The directivity D of an antenna is defined as the radiation intensity in a given direction from the antenna to the radiation intensity averaged over all directions [19]

$$D = \frac{U}{U_0} = \frac{4\pi U}{P_{\text{rad}}}, \tag{2.2}$$

where U is the radiation intensity in W/unit solid angle and U_0 is the radiation intensity of

an isotropic source in W/unit solid angle given as $P_{\text{rad}}/4\pi$. The directivity of the antenna was evaluated by TU Wien in an anechoic chamber. It was measured for different configurations for an azimuth angle $\phi \in [-180°, 180°)$ and polar angle $\theta \in [0°, 140°]$ in one degree steps. Figures 2.6 to 2.8 illustrate the Mercator's projection of the directivity of the antenna for different configurations. Figure 2.5 illustrates the orientation of the ESL in the coordinate system of the measurement. The display of the ESL is pointing into the positive x-direction while the left to right direction of the displayed text points into the positive y direction. The azimuth angle is defined in the x-y plane where the x-axis has an azimuth angle of 0° and the y-axis has an azimuth angle of 90°. The polar angle is measured from the z-axis. A single ESL exhibits a higher directivity for an azimuth angle between $\phi \in [-180°, 0°)$. To investigate the effect of the coupling of densely spaced ESLs, the transmitting ESL was placed between two non operating ESLs and the directivity was measured. The pattern of the directivity becomes more symmetric in comparison to a stand alone ESL. Finally, the directivity of an ESL attached to a shelf was determined. This measurement addresses the circumstance that most of the ESLs are attached to a shelf. It can be seen that the directivity becomes more dominate in the positive x-direction. It should be noted that the directivity for an ESL mounted onto a shelf depends strongly on the shelf due to coupling and reflection effects.

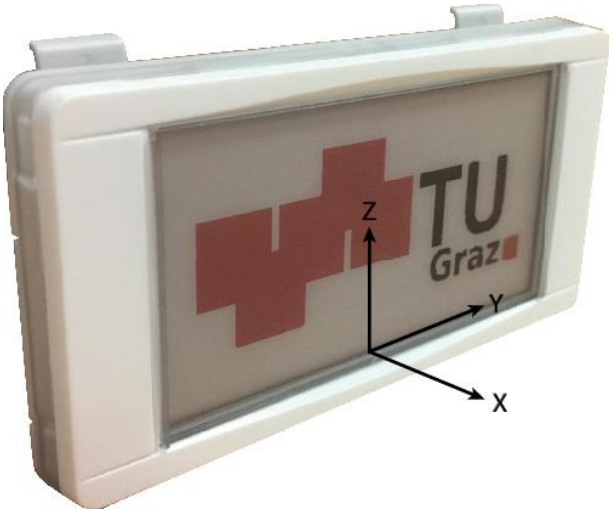

Figure 2.5: Orientation of an ESL in the coordinate system

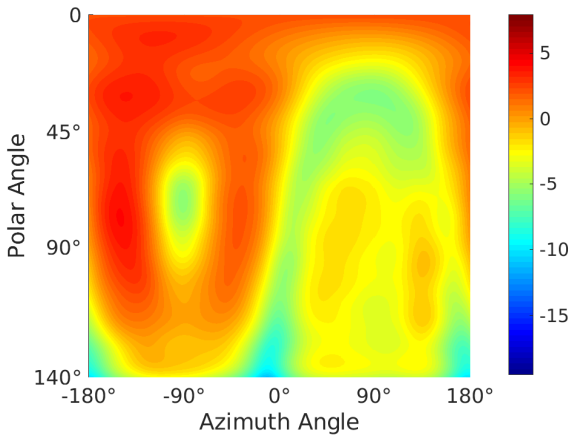

Figure 2.6: Mercator's projection of the directivity in dB of a single ESL without shelf

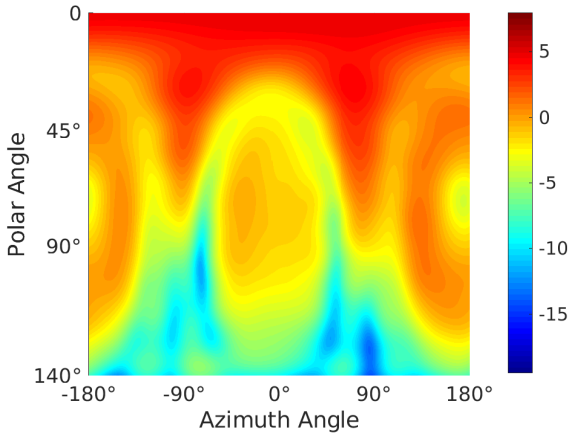

Figure 2.7: Mercator's proejection directivity in dB of 3 closely spaced ESLs without shelf

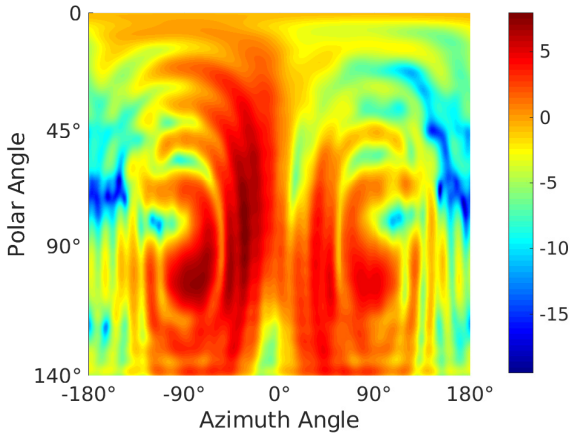

Figure 2.8: Mercator's proejection of the directivity in dB of a ESL mounted on a shelf

Neither the S_{11}-parameter nor the directivity takes the efficiency of the antenna into account

and has to be addressed by other measurements.

2.2.2 Link conditions

In Section 2.1.1, the possible link conditions for the given layout were presented. From the five possible link conditions, four were investigated in this measurement campaign. Two out of the nine modified ESLs were used as transmitters (Tx) while the seven remaining ESLs were used as receivers (Rx). The two transmitters (Tx) were placed on shelves S7 and S8, respectively. The Tx ESLs were placed at three different heights (0.5 m, 1 m and 1.5 m) and at each height at ten different positions. Each positions were spaced equally by 10 cm. The single link conditions were investigated by placing the receiver on appropriate shelves. The position of the Tx ESLs is indicated by the red and blue squares in Figures 2.9 - 2.12. From all Tx positions, measurements to all receiver (Rx) ESLs were made. A detailed description of the positions of the single ESLs can be found in Appendix C.

NLOS, facing

The *NLOS, facing* link condition was investigated by placing the seven Rx ESLs on shelves S1 and S2. The LOS link is obstructed by the shelves S3 to S6 as illustrated in Figure 2.9.

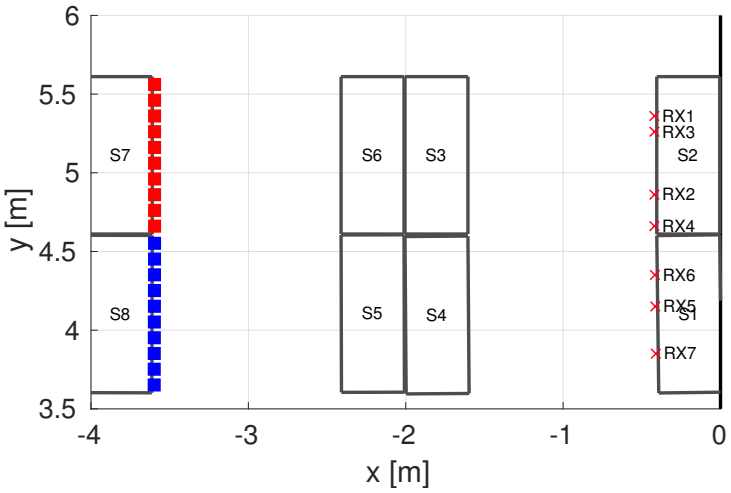

Figure 2.9: Layout of the NLOS, facing scenario

NLOS,aligned

To analyze this link condition, the seven Rx ESLs were placed on shelves S3 and S4, see Figure 2.10. The LOS link is not only obstructed by the shelves S3 to S6, but the Rx ESLs also experience a low directivity in the LOS direction towards the Tx.

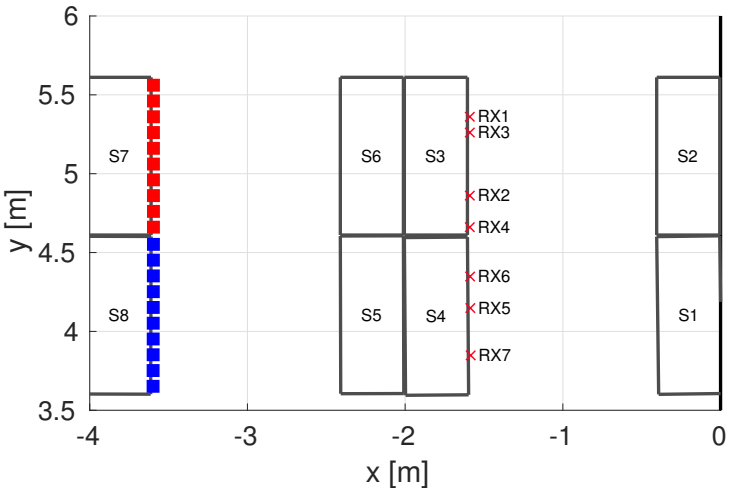

Figure 2.10: Layout of the NLOS, aligned scenario

LOS,facing

The *LOS, facing* link condition was investigated in two measurements. This link condition was evaluated in more detail since it features an unblocked LOS link and therefore could be exploited for localization tasks. For this reason, the links from the different transmitter positions to 14 distinguishable Rx ESL positions were evaluated. These 14 measurements were carried out in two consecutive runs, by measuring 7 position in each run, see Figures fig:LOS1 and 2.12.

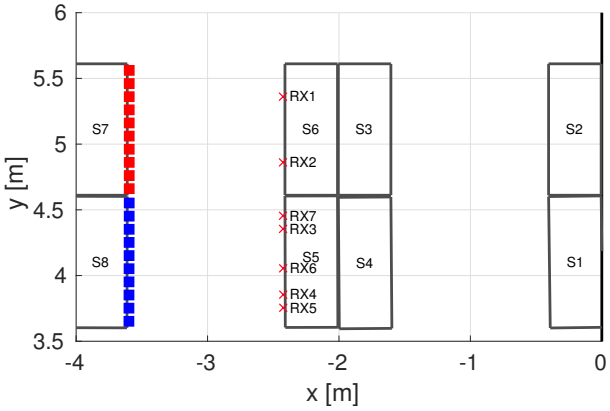

Figure 2.11: Layout of the first LOS scenario

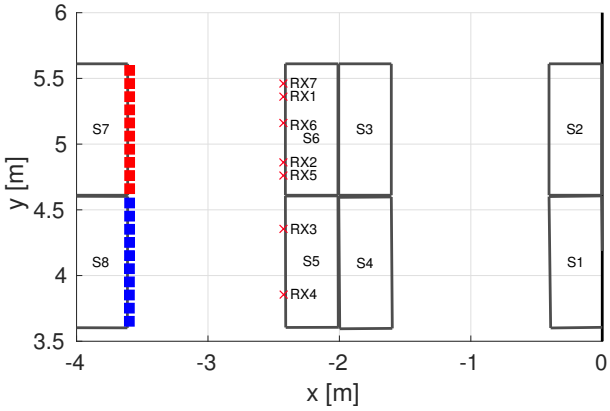

Figure 2.12: Layout of the second LOS scenario

Two more additional measurements were carried out for this kind of link condition. One measurement addressed the coupling effects between closely space Rx ESLs. Therefore, Rx ESLs were placed in groups on shelves S5 and S6, see Figure 2.13.

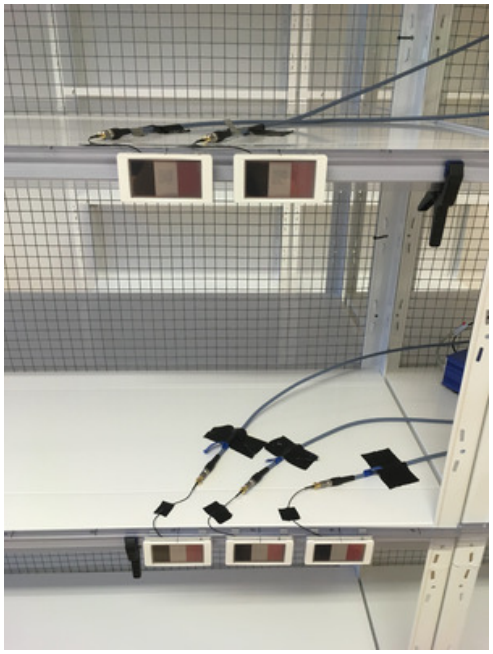

Figure 2.13: Grouping of receiver ESLs

LOS, same shelf

The *LOS, same shelf* was evaluated by placing the Tx and Rx ESLs on shelves S5 and S6. The measurements were carried out in two steps. In the first step, the Rx ESLs were uniformly distributed on the shelves while the Tx ESL positions were varied. In the second step the Rx ESL were placed in groups and the measurement for different Tx ESL positions repeated.

2.3 Measurement Campaign - Electronic Shelf Label

2.3.1 Measurement Setup

32 regular ESLs were used for this measurement campaign. The used ESLs were identical in terms of hardware to regular ESLs deployed in shops. An adopted software was used for the purpose of the measurement campaign. The accuracy of the RSSI values of the transceiver was evaluated by TU Wien in [20]. It has become apparent that the RSSI values are slightly biased. Moreover, the bias is a function of the RSSI value itself. The source of this RSSI dependent bias was found in the Automatic Gain Control (AGC). To mitigate this effect, a fixed AGC value was used within the measurement campaign. A drawback of the fixed AGC value is that the amplifier enters saturation, hence the RSSI is not reported for values above 34 dBm. The ESLs were controlled by an access point which sets one ESL into receive mode while all other are set as transmitters. The transmitter ESLs send messages consecutively to the receiver ESL which collects the RSSI values from all transmitter ESLs. After 5 cycles, where each transmitter sends one message, another ESL will be assigned as receiver according to a round robin principle and the procedure of collecting RSSI values starts again. After each of the 32 ESL was assigned once as receiver, the overall procedure starts again. Within this measurement campaign, each label was assigned 4 time as a receiver and could collect in total up to 20 messages from each ESL. A description of the measurement procedure can be found in Appendix C.2. The link condition between ESLs can be determined by their position in combination with the layout. In order to obtain comparable results, the ESLs were placed in a similar fashion as for the channel sounder

measurement campaign. Four ESLs were placed on each shelf. A detailed description of the placement can be found in the Appendix C.1. Figure 2.14 depicts the link conditions between each pair of ESLs. Table 2.2 describes the corresponding colormap.

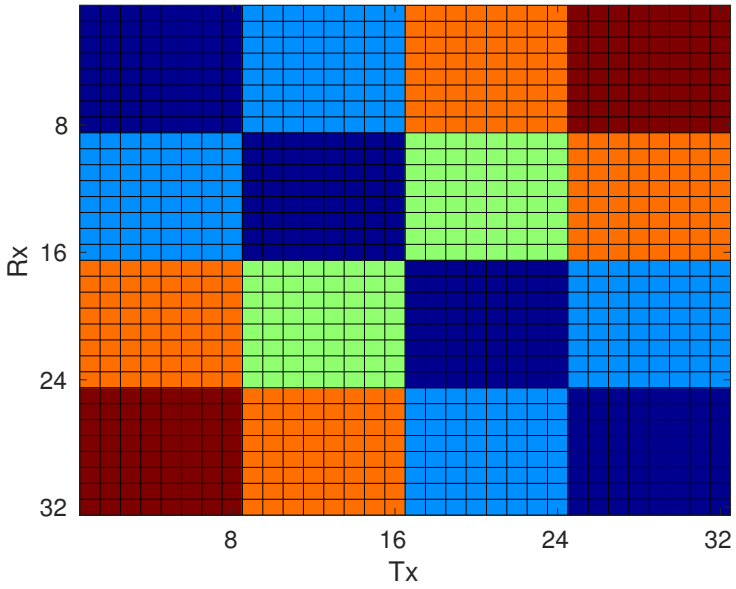

Figure 2.14: Overview of the link conditions between pairs of ESL

Color	Link Condition
dark blue	LOS, same shelf
light blue	LOS, facing
orange	NLOS, aligned
light green	NLOS, back to back
dark red	NLOS, facing

Table 2.2: Corresponding color map

3 Channel Characterization

Wireless channels are dominated by multipath propagation of the transmitted signal. This is especially true for indoor channels where a vast amount of interacting objects (IO) are present. The propagation effects which are introduced by these IOs are reflection, diffraction and scattering of the transmitted signal. The path length for multipath components are different and cause a delay dispersion of the received signal. Under this condition, two different effects on the transmitted signal can be distinguished depending on the bandwidth of the transmitted signal. First, if the bandwidth reciprocal is much longer than the delay spread of the channel, then no dispersion occurs at all. The received signal is thus a sum of scaled replicas of the transmitted signals which interfere and cause a change in amplitude and phase. This case is referred as flat fading and is modelled by narrowband models. Second, if the bandwidth reciprocal is smaller than the delay spread of the different multipath components. Such a scenario can be described by wideband models. Both cases are described in the following section shortly. Literature about channel models can be found in [16, 21–23].

3.1 Channel Models in Literature

3.1.1 Narrowband Model

Narrowband models assume that the channel transfer function is constant over the bandwidth of the transmitted signal and therefore they experience frequency flat fading. Narrowband propagation is mainly governed by three different effects. The first effect is path loss which addresses the decrease of the received power with the separation, mainly based on free space loss. The second phenomenon is shadowing which is introduced by IO which attenuate the transmitted signal when it has to pass through or around an object. The first two effects are referred to as large scale fading while the third effect addresses the random fluctuations of the signal power over short distances (in the order of wavelengths) which is caused by the interference of multipath components at the receiver position. In Figure 3.1, the received power is depicted as a function of the transmitter-receiver distance which is composed of the three mentioned effects.

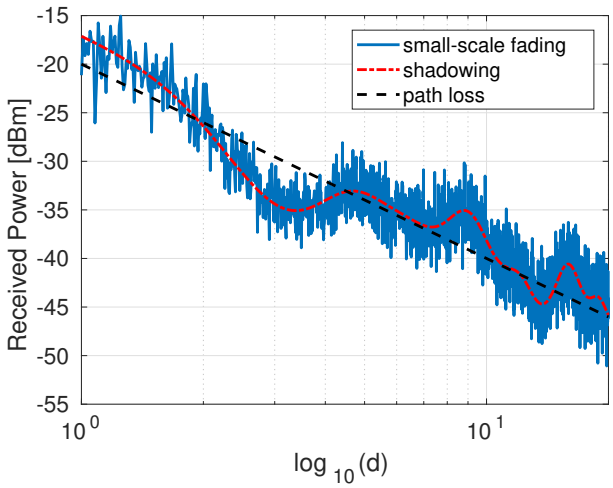

Figure 3.1: Effect of fading

Statistical Description

Due to the large amount of multipath components in indoor environments, a deterministic channel model is often not tractable. Therefore, the received amplitude is described by a probability distribution. The Ricean distribution is used for a link with a strong dominant component, typically but not necessarily an LOS component. The Ricean distribution is usually described by the Ricean K-factor which is the ratio of the power of the dominant component to the power of the remaining multipath components. For links without a dominant component, the Rayleigh distribution is used to model the amplitude distribution, which is a special case of the Ricean distribution with Ricean K-factor equal to zero. The probability density function (PDF) of an amplitude r with Ricean distribution is given as:

$$f_r(r) = \frac{r}{\sigma^2} \cdot exp\left(-\frac{r^2+s^2}{2\sigma^2}\right) I_0\left(\frac{rs}{\sigma^2}\right) \quad 0 \leq r < \infty, \tag{3.1}$$

with non-centrality parameter $s \geq 0$ and scale parameter $\sigma > 0$. The non-centrality parameter s reflects the amplitude of the dominant component while the scale parameter σ refers to the sum of the amplitudes of the scattered components. $I_0(\cdot)$ denotes the 0th order modified Bessel function of the first kind. Moreover, the Ricean K-factor is given as:

$$K = \frac{s^2}{2\sigma^2}. \tag{3.2}$$

The PDF of the power p of a Ricean fading channel is described by a non-central chi squared distribution with two degrees of freedom and can be described in terms of the Ricean K-factor as [23]:

$$f_p(p) = \frac{K+1}{\Omega_p} exp\left(-K - \frac{(K+1)\,p}{\Omega_p}\right) I_0\left(2\sqrt{\frac{K\,(K+1))\,p}{\Omega_p}}\right) \quad 0 \leq p < \infty, \tag{3.3}$$

where $\Omega_p = s^2 + 2\sigma^2$ describes the total power. Figure 3.2 illustrates the importance of the K-factor for ranging tasks. A high K-factor reduces the spread of the power and therefore ranging would give more accurate results.

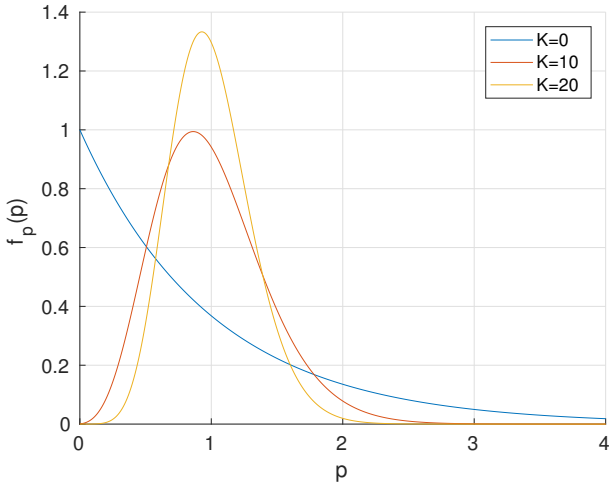

Figure 3.2: PDF of p for different values of K and $\Omega_p = 1$

The PDF of an amplitude r which is Rayleigh distributed is given as [16]:

$$f_r(r) = \frac{r}{\sigma^2} \cdot exp\left(-\frac{r^2}{2\sigma^2}\right) \quad 0 \leq r < \infty, \tag{3.4}$$

where $\sigma > 0$ is the so called scale parameter. The power p of a Rayleigh distributed amplitude r which is represented by the squared amplitude can be found to be exponentially distributed [23] with PDF:

$$f_p(p) = \frac{1}{\sigma^2} exp\left(\frac{-p}{\sigma^2}\right) \quad 0 \leq p < \infty. \tag{3.5}$$

This fact is addressed in Figure 3.2 for K = 0.

3.1.2 Wideband Models

Another way to describe the wireless channel is in terms of a linear time-variant system. The received signal is therefore given as [16]:

$$y(t) = \int_{-\infty}^{\infty} x(t-\tau)h(t,\tau)d\tau, \tag{3.6}$$

where $x(t)$ is the transmitted signal. The CIR $h(t,\tau)$ can be modelled by a tapped delay line

$$h\left(t,\tau\right) = \sum_{i=0}^{N-1} \alpha_i(t)\delta\left(\tau - \tau_i(t)\right) \mathrm{e}^{j\theta_i(t)} \tag{3.7}$$

The first tap is considered as the direct path between a transmitter and receiver in case of an unobstructed link while the following taps model the multipath components for different propagation paths. Because of the stochastic nature of the multipath components, it is preferable to describe the channel by means of its Auto Correlation Function(ACF):

$$R_h(t,t',\tau,\tau') = \mathbb{E}\{h^*(t,\tau)h(t',\tau')\} \tag{3.8}$$

Different quantities like the coherence bandwidth, time or distance can be derived from the ACF and its corresponding Fourier transforms. Specific assumptions about the wireless channel can be

made in order to obtain a simplified model. Instances of such assumptions are the widely used Wide-Sense Stationarity (WSS) and Uncorrelated Scattering (US) assumptions which givein combination the WSSUS assumption [16].

Power Delay Profile

Another commonly used way to describe the wideband channel is by the power delay profile (PDP) which is given by the squared magnitude of the CIR:

$$S(\tau) = \lim_{T\to\infty} \frac{1}{2T} \int_{-T}^{T} |h(t,\tau)|^2 dt. \tag{3.9}$$

The PDP describes the received power in the delay domain. The moments of the PDP are of special interest since it can be shown that the normalized second-order moment which is known as the root mean square (rms) delay spread is proportional to the delay dispersion of the channel [16]. The rms delay spread is given by:

$$\tau_{\text{rms}} = \sqrt{\frac{\int_{-\infty}^{\infty} (\tau - \tau_{\text{mean}})^2 S(\tau) d\tau}{\int_{-\infty}^{\infty} S(\tau) d\tau}}, \tag{3.10}$$

where τ_{mean} is the mean excess delay given by:

$$\tau_{\text{mean}} = \frac{\int_{-\infty}^{\infty} \tau S(\tau) d\tau}{\int_{-\infty}^{\infty} S(\tau) d\tau}. \tag{3.11}$$

The rms delay spread τ_{rms} and the coherence bandwidth B_{coh} are related for WSSUS channels according to [16]:

$$B_{\text{coh}} \gtrsim \frac{1}{2\pi\tau_{\text{rms}}}, \tag{3.12}$$

where the coherence bandwidth B_{coh} is defined as the bandwidth for which the spaced frequency correlation function $R_H(\Delta t = 0, \Delta f)$ of the channel drops 3 dB from its value at $\Delta f = 0$. The coherence bandwidth is of paramount importance if frequency diversity is exploited.

Power Delay Profile Models

The PDP is usually modelled as composition of one or more specular components and diffuse multipath components [24, 25]. The delay power spectrum of the diffuse multipath components follows an exponential decay. In Figure 3.3, a PDP with one dominant LOS component and an exponentially decaying diffuse part at the tail of PDP is depicted which is commonly referred to as *spike-plus-exponential* shape.

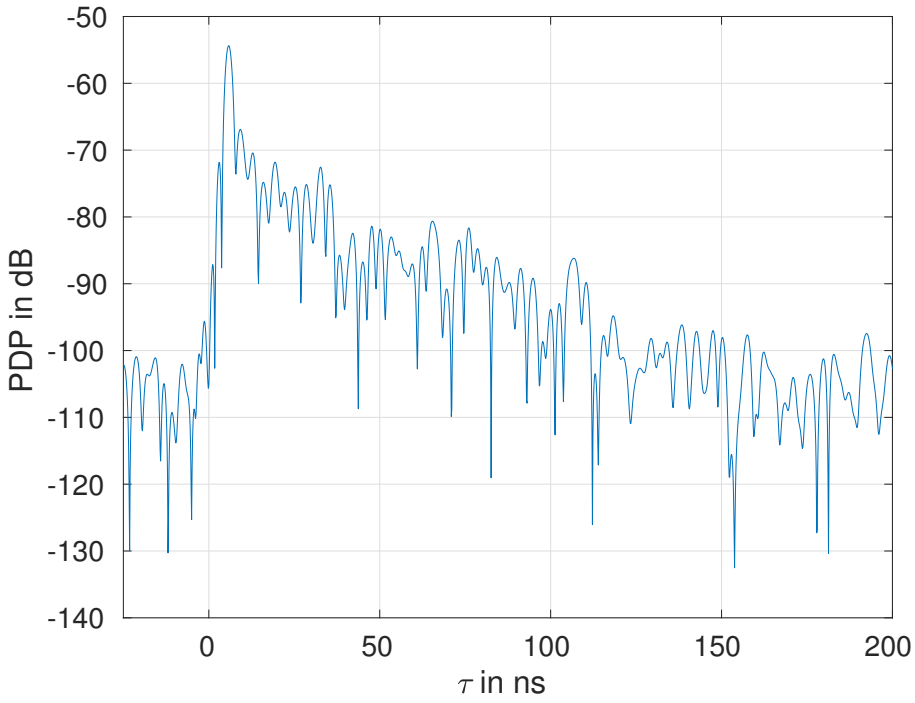

Figure 3.3: Example of a PDP

Saleh and Valenzuela carried out measurements for indoor scenarios and described the indoor channel by clusters of rays. Within each cluster, the power decays exponentially while the peak power of the clusters also decays exponentially with a longer decay time constant. The arrival of clusters was modelled by a Poisson arrival process [26]. In [27] the concept of Room Electromagnetics (REM) is introduced. It is based on the analogy to room acoustics where the reverberation time of the diffuse field depends on the volume, surface and absorption coefficient of the room and objects within. The model was validated in [28] and [29] while in [30] the distance dependency of the model was evaluated. One important aspect is that the tail of the PDP decays exponentially with the same time constant, independent of the transmitter-receiver separation [31].

3.2 Evaluation of the measurements

3.2.1 Narrowband Results

Narrowband results are obtained by performing pulse shaping of the measured CIR with a raised cosine pulse with a pulse duration of $T_p = 1\mu$s and a roll-off factor of $\beta = 0.6$. All narrowband measurements were carried out for the eleven channels of the ESL with center frequencies given in Table A.1.

Path Loss

The received power at a given distance d for free space propagation can be described according to Friis equation as:

$$P_{rx}(d) = \frac{P_{tx} D_{tx} D_{rx} \lambda^2}{(4\pi)^2 d^2}, \tag{3.13}$$

where P_{tx} is the transmitted power, D_{tx} and D_{rx} are the directivities of the transmitter and receiver antennas, respectively and λ is the wavelength of the transmitted signal. Moreover, the path loss PL in dB is defined according to [21] as:

$$PL = 10 \log_{10} \left(\frac{P_t}{P_r} \right) \tag{3.14}$$

where P_t is the transmitted power and P_r is the received power. Equation (3.14) is only valid in the far field of the antenna. The path loss is a relative measure to the transmitted power and can thus be used independently of the measured power. Figure 3.4 illustrates the empirical cumulative distribution function (CDF) of the path loss for the four evaluated link conditions.

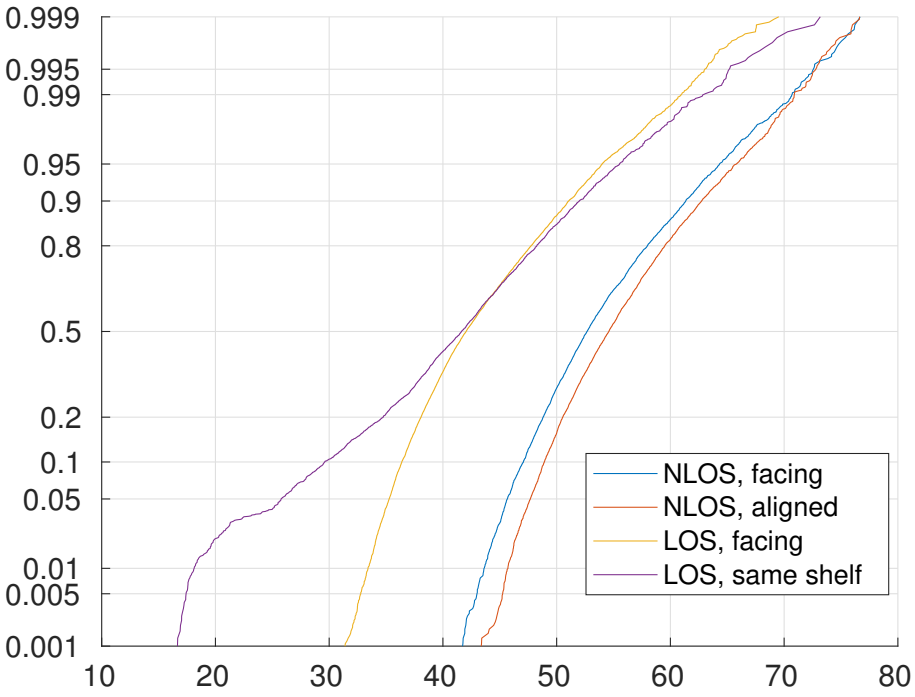

Figure 3.4: Empirical CDF of the path loss for the different scenarios for channel sounder measurement campaign

It can be seen that the distribution of path loss is almost the same for the two evaluated *NLOS* link conditions. For the *LOS, same shelf* link scenarios it can be seen that 10% of the links experience a path loss less than 30 dB while for the range between 40 and 70 dB both *LOS* links show the same distribution, corresponding to approximately 50% of those measurement. The divergence at the lower range can be explained by the close spacing of the ESLs on a shelf (10 cm). Based on the CDFs it can be seen that the distributions of the path loss values can be divided into three groups. The first group is defined by closely spaced ESLs on the same shelf. The second group defines links between ESLs on the same shelf or in the same corridor which are spaced by more than ca. 0.5 m apart since they are not distinguishable. The third group is given by ESLs placed in two different corridors. These links share almost the same statistics and therefore it can be assumed that the directivity does not have an influence.

Frequency Diversity

Each of the eleven channels is affected in a different way by multipath propagation and therefore experiences a different channel gain (assuming the channels are not correlated). A possible way to diminish small scale fading caused by multipath propagation would be to average the experienced received power at the different channels. In Figure 3.5, the empirical CDFs of

the averaged path losses are illustrated. Deep fades which are characterized by high path loss values are mitigated. The maximum experienced path loss values are reduced by more than 10 dB for each link condition. The statistics of the path loss for the *NLOS* links become normal distributed (given by a straight line in this representation). Such assumptions are made for log normal shadowing models [21].

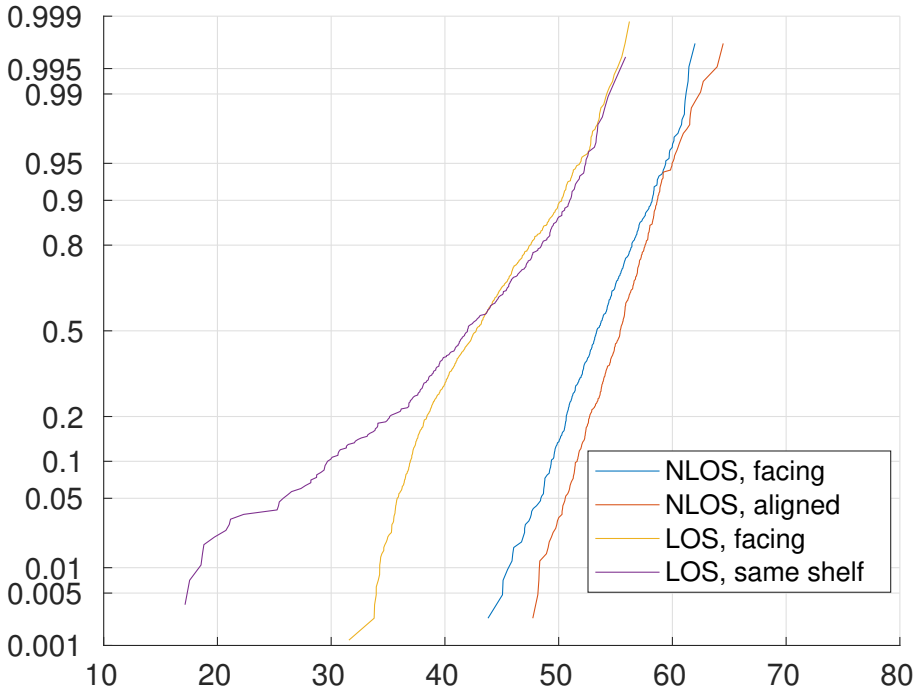

Figure 3.5: Empirical CDF of the averaged path loss

Spatial distribution of the path loss

Localization algorithms, based on ranging, aim to determine the position of an Rx based on distance estimation to different Tx. Moreover, the question arises how accurate RSS values are for ranging in the given setup. A popular model for RSS-based ranging is the log normal shadowing model which is given as [21].

$$P_r(d) = P(d_0) - 10nlog_{10}\left(\frac{d}{d_0}\right) + X, \quad X \sim \mathcal{N}(0, \sigma^2) \tag{3.15}$$

where $P(d_0)$ is the power at a reference distance d_0. The second term addresses the path loss and n is the so called path loss exponent which depends on the environment and is chosen typically in the range from 1.6 to 6 [21]. The random variable X models the shadowing and is modelled by a zero mean normal distribution in the log domain. The first two terms describe the mean of the received power in dB. Within the *LOS, facing* measurement varies the distance between pairs of Tx and Rx ESLs from 1.2 m to 2.3 m. Assuming a path loss coefficient of $n = 2$, a PL variation of about 6.3 dB would be expected from the closest to the most distant Tx-Rx distance. Figure 3.6 and 3.7 present two situations where such a variation is reproduced. The red line indicates the possible range for Tx ESLs on the shelf.

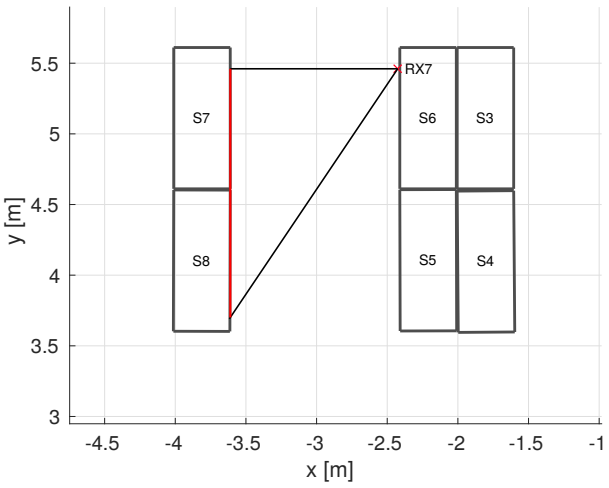

Figure 3.6: Covered area of Rx ESL 7

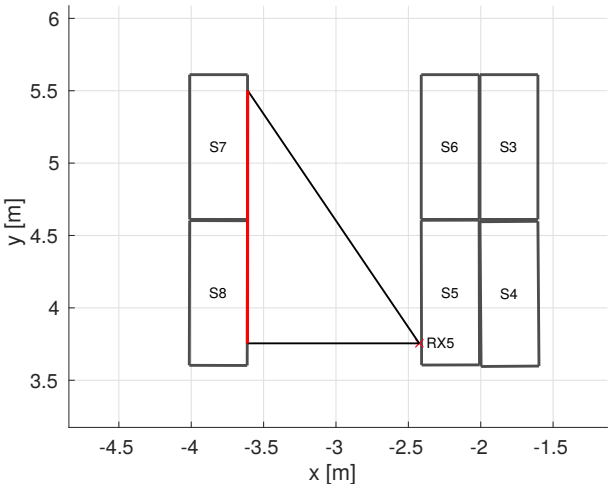

Figure 3.7: Covered area of RX ESL 5

The measured distribution of the path loss from 60 positions on shelves S7 and S8 is illustrated in Figures 3.8 and 3.9. Rx ESL 5 captures the path loss distribution for Tx ESLs placed at an azimuth angle smaller than 0° with respect to the Rx ESL while Rx ESL 7 captures the path loss values experienced for angles greater than 0° . It can be seen that the distance is not the governing factor for such links. Links to the Rx ESL 5 experience a much lower path loss than these for Rx ESL 7. The path loss varies for both Rx ESLs in the range of about 20 dB.

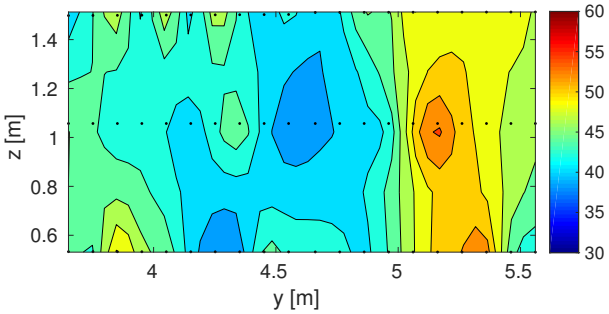

Figure 3.8: Path loss in dB experienced from Rx ESL 7 from the different Tx ESL positions

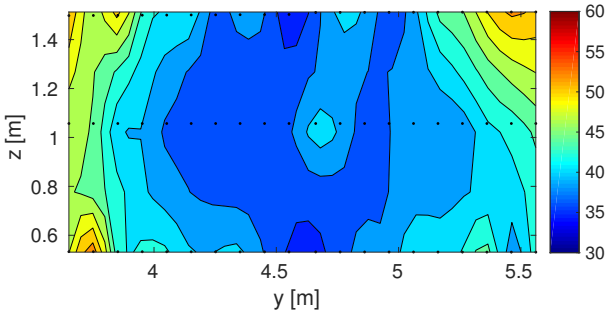

Figure 3.9: Path loss in dB experienced from Rx ESL 5 from the different Tx ESL positions

Path Loss as a function of distance

Figures 3.8 and 3.9 address the spatial distribution of the path loss value for the *LOS, facing* link condition. On the other hand, it is of interest how accurate the path loss reflects the distance separation over a wider distance range. Figure 3.10 depicts the dependency of the RSS value as a function of the distance. A clear path loss/distance correlation can only be seen for closely spaced ESLs which are not separated by more than 0.5 m. For larger distances, no clear distance path loss dependency is observable.

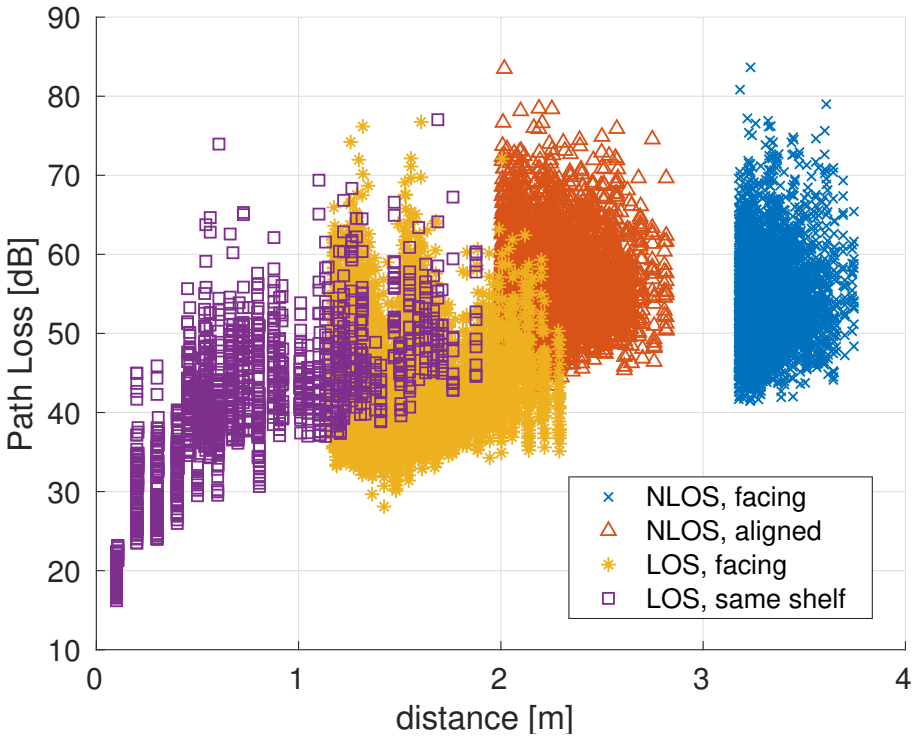

Figure 3.10: Path loss versus distance

3.2.2 Amplitude Distribution

The amplitude distribution can be inferred from the path loss distribution. Section 3.1.1 addressed the amplitude distribution of multipath channels which we can assume to be either Rayleigh or Ricean distributed. The Rayleigh distribution is a special case of the Ricean distribution with a Ricean K-factor equal zero (which is equivalent to a non-centrality parameter s equal to zero). Due to this fact, a Ricean distribution can be used for distribution fitting to the data in both cases. Table 3.1 provides the estimated parameters of the fitted Ricean distribution. Both *NLOS* and the *LOS, facing* links show a small Ricean K-factor. For the *NLOS* links this is expected, since the LOS link is blocked and no strong component is present. The result for the *LOS, facing* link is unexpected since a dominant component could be expected due to unblocked LOS links.

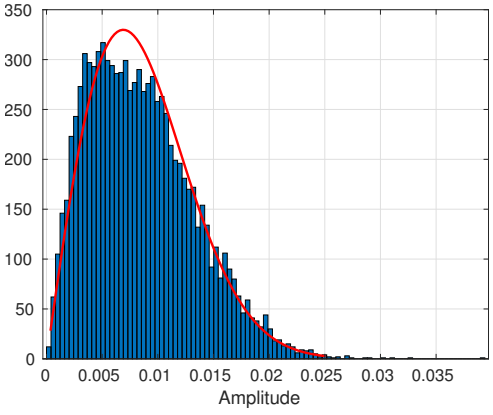

Figure 3.11: Amplitude distribution for LOS, facing *links*

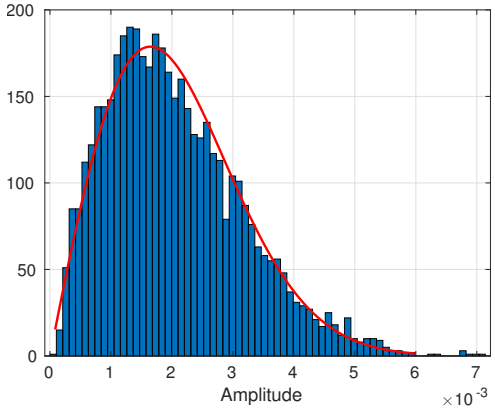

Figure 3.12: Amplitude distribution for NLOS, aligned *links*

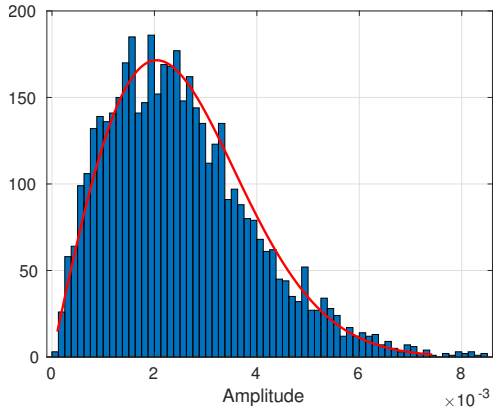

Figure 3.13: Amplitude distribution for NLOS, aligned *links*

Scenario	s	σ	Ricean K-factor
LOS, facing	7.244e-4	6.9e3	-22.56 dB
NLOS, aligned	8.236e-7	1.6e3	-66 dB
NLOS, facing	9.018e-7	2e3	-70.10 dB

Table 3.1: Parameter of the fitted Ricean distribution

3.3 Wideband results

The CIRs for the wideband measurements were evaluated in the complex baseband representation of the real valued CIRs obtained from the channel sounder. Therefore, a Hilbert transformation was applied and the resulting analytical CIR was shifted to the baseband by the center frequency of 2.4GHz. To limit the bandwidth of the CIR to the according antenna bandwidth, pulse shaping was performed in the post processing step of the measured CIRs. The pulse shaping was done in frequency domain by multiplying the channel transfer function (CTF) which is the Fourier transform of the CIR with the Fourier transform of a raised cosine pulse with pulse duration $T_P = 5ns$ and roll-off factor $\beta = 0.5$. The band-limited complex low pass representation of the CIR is therefore given as [32]:

$$h\left(\mathbf{x}_{tx}, \mathbf{x}_{rx}, \tau\right) = \sum_{n=0}^{N} h_n\left(\mathbf{x}_{tx}, \mathbf{x}_{rx}\right) \cdot w\left(\tau - nT_s\right), \tag{3.16}$$

where $w(t)$ is the window (raised cosine pulse) and h_n are the complex path gains and T_s the sampling rate. The channel is assumed to be stationary during the measurement campaign since no moving IO were present. The CIR is therefore described as a function of the transmitter position $\mathbf{x}_{tx}$ and receiver position $\mathbf{x}_{rx}$. The band limitation of the ESL antennas reduces the capability of resolving the multipath components. Moreover, each tap of the tapped delay line model is the sum of several different multipath components. In Equation (3.7), the single multipath components are given with an arbitrary arrival time which is not valid for the measured CIR since the sampling points are equally spaced in time.

3.3.1 Power Delay Profile

The instantaneous PDP of a single channel realization is given as:

$$S\left(\mathbf{x}_{tx}, \mathbf{x}_{rx}, \tau\right) = \left|h\left(\mathbf{x}_{tx}, \mathbf{x}_{rx}, \tau\right)\right|^2. \tag{3.17}$$

Averaged Power Delay Profile

The averaged power delay profile is obtained by averaging the PDP over different transmitter and receiver positions

$$\overline{S}\left(\tau\right) = \frac{1}{N_{tx}, N_{rx}} \sum_{i=1}^{N_{tx}} \sum_{i=1}^{N_{rx}} \left|h\left(\mathbf{x}_{tx}, \mathbf{x}_{rx}, \tau + \frac{1}{c}\|\mathbf{x}_{tx} - \mathbf{x}_{rx}\|\right)\right|^2, \tag{3.18}$$

where $\|\mathbf{x}_{tx} - \mathbf{x}_{rx}\|$ is the distance between the Tx and Rx. A requirement for the averaging is ergodicity. This assumption is not valid for *LOS* links since the antenna with its strongly varying directivity is considered part of the channel. However, for comparisons of the diffuse part, the WSS assumption can be assumed valid since the antenna directivity in a random field is unity. The instantaneous PDPs were aligned in the delay domain prior to averaging. Therefore, each instantaneous PDP was shifted in the negative delay direction by the propagation time of the LOS component. The aligning of the instantaneous PDP reduces the "smearing" of the APDP due to averaging of the PDPs with different path lengths of the direct path. The averaging includes all measured Tx and Rx positions. Figures 3.14 and 3.15 illustrate the APDPs for the two LOS scenarios. Both *LOS* link conditions are dominated by a strong LOS component. Beside the LOS component three strong components are present. The additional components were identified to be artefacts introduced by non-linear effects of the measurement system for high values of the received power. By neglecting these artefacts it can be seen that the APDP follows the commonly used *spike-plus-exponential* shape with one dominant LOS component and exponentially decaying tail of the diffuse multipath.

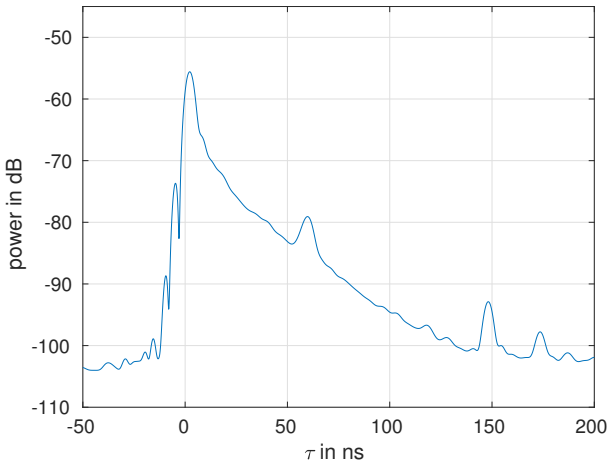

Figure 3.14: APDP of the LOS, facing *link*

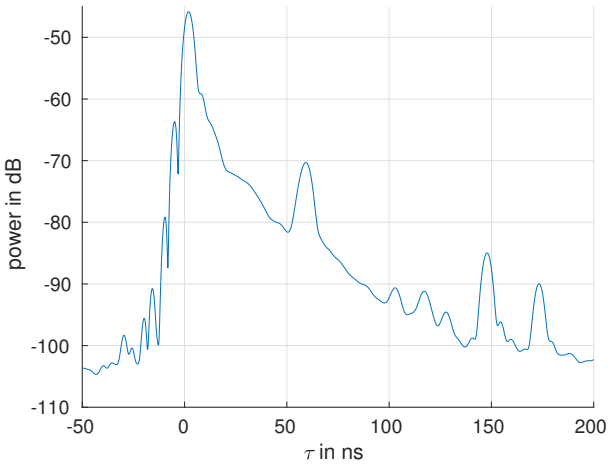

Figure 3.15: APDP of the LOS, same shelf *link*

Unlike for the *LOS* link conditions, in the *NLOS* link condition no strong components are visible. The maximum power is slightly different while the decaying time is the same for both evaluated *NLOS* link conditions.

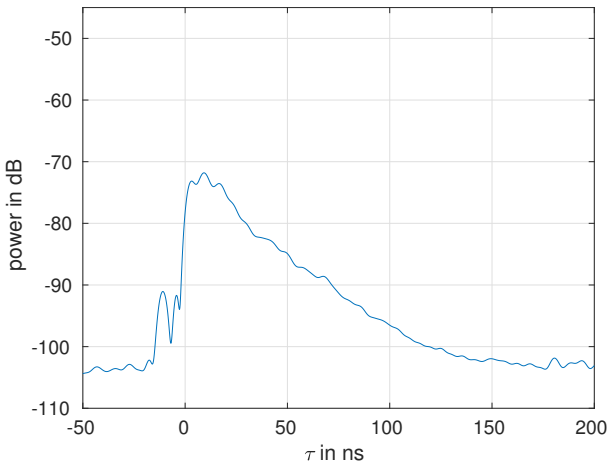

Figure 3.16: APDP of the NLOS, facing *link*

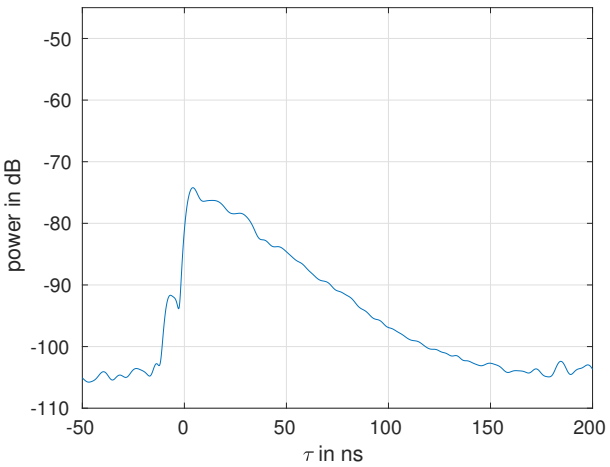

Figure 3.17: APDP of the NLOS, aligned *link*

No significant change of the APDP can be observed in case of groups of Rx ESLs. The coupling effects of the shelf dominates the overall directivity. This observation is valid for the two LOS links for which measurements of Rx ESL groups were performed. Figure 3.18 provides a comparison between an APDP obtained from measurements in RX groups as well as for widely spaced Rx ESLs.

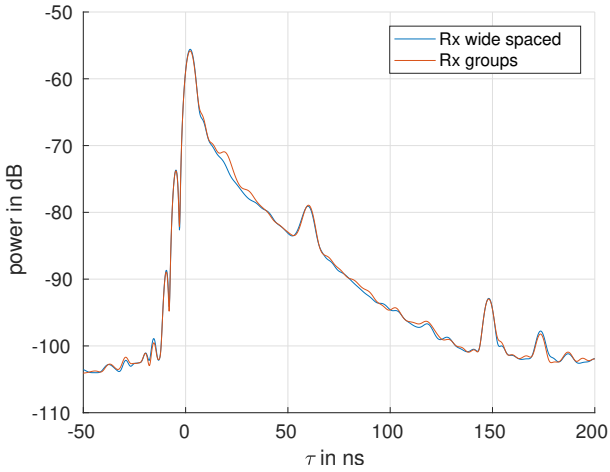

Figure 3.18: APDP for receiver ESL groups for a LOS, facing *scenario*

K-factor

Another parameter which can be computed from the instantaneous PDP is the K_{LOS}-factor which is defined in a similar fashion as for the Ricean distribution:

$$K_{\mathrm{LOS}} = \frac{P_{\mathrm{LOS}}}{P_{\mathrm{NLOS}}}. \tag{3.19}$$

The K_{LOS}-factor describes the ratio between the power of the LOS component to the scatter components and is therefore an important parameter for ranging tasks. It is estimated by subtracting the estimated power of the direct path from the total power:

$$K_{\mathrm{LOS}} = \frac{P_{\mathrm{LOS}}}{P_{\mathrm{total}} - P_{\mathrm{LOS}}}. \tag{3.20}$$

The estimation of the K_{LOS}-factor is done in three steps. In the first step, the noise floor is estimated and only the part of the PDP which exceeds the noise floor significantly is extracted. In the next step, the LOS-component is estimated. Therefore, the amplitude and phase of the received LOS pulse are estimated by projecting the transmitted pulse onto the received signal. In the following step, the weighted version of the transmitted is pulse subtracted from the received signal. The K_{LOS}-factor is then the ratio between the energy of the LOS component and the energy of the difference signal which is considered to be the NLOS signal. Figures 3.19 and 3.20 exemplify this approach. Figure 3.19 illustrates an instance of an instantaneous PDP and Figure 3.20 shows the separation into the LOS and NLOS parts of the PDP.

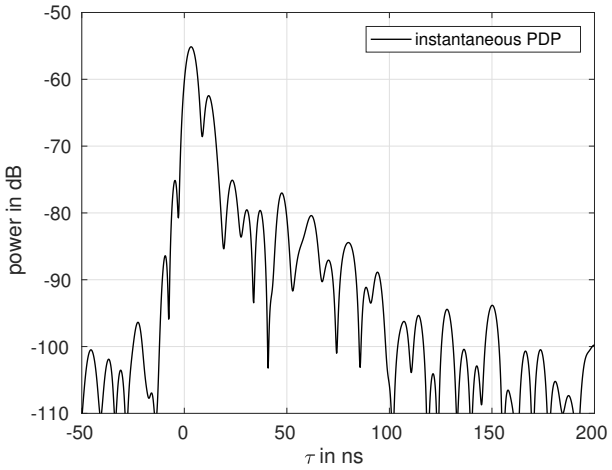

Figure 3.19: Instance of an instantaneous PDP

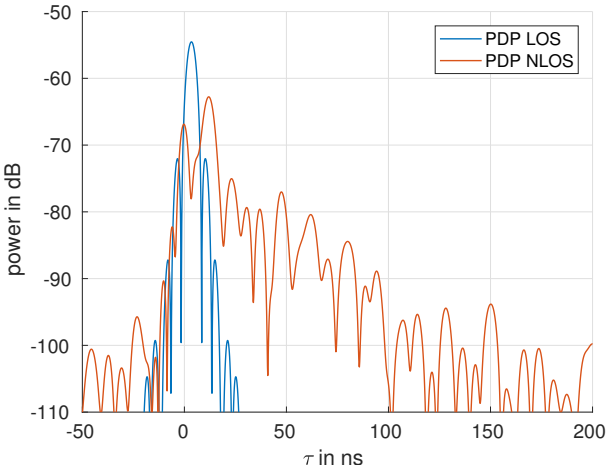

Figure 3.20: Separation into LOS and NLOS PDP

The empirical CDF of the estimated K_{LOS} for the different link conditions is depicted in Figure 3.21. It shows that the LOS links up to 80% of the K_{LOS}-factors are larger than 0 dB. The median of the K_{LOS}-factor for the *NLOS* scenarios drops by 10 dB compared to the *LOS, facing* link. Up to 90% of the *NLOS* links are below 0 dB meaning that the diffuse part is dominant.

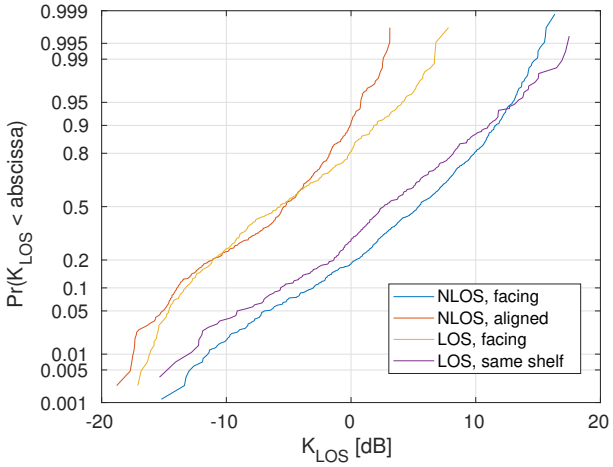

Figure 3.21: Empirical CDF of the K_{LOS}-factor for the different link conditions

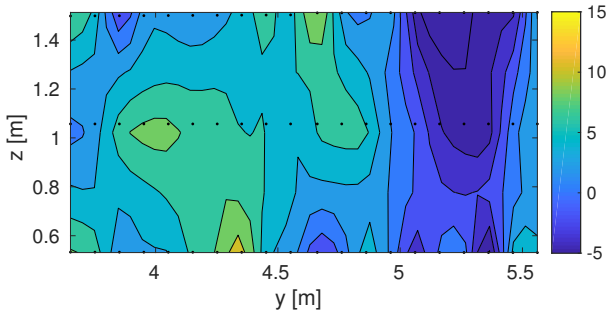

Figure 3.22: K_{LOS} from Rx ESL 7 from the different Tx ESL positions

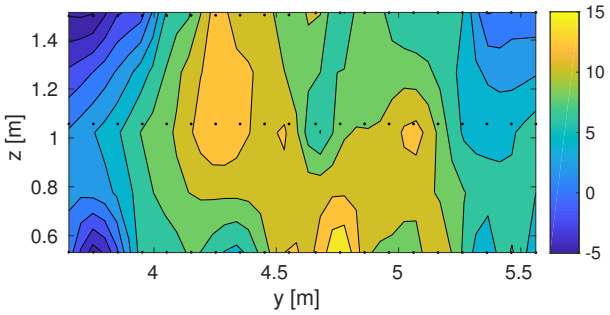

Figure 3.23: K_{LOS} from Rx ESL 5 from the different Tx ESL positions

It can be seen that the K_{LOS}-factor shows a strong direction dependency. Due to the parallel arrangement of the shelves, the Tx and Rx ESLs experience the same azimuth angle for a given link. High K_{LOS} values can be observed for links with an azimuth angle of -20° to -45°. Such links can be found for Rx ESL 5 and Tx ESLs placed at y coordinate in the range of 4.25 to 5 m. On the other hand, links with a low K_{LOS}-factor can be found in both cases for links with an azimuth angle of about 0°. The strong angle dependency of the K_{LOS}-factor is a result of the overall directivity including Tx and Rx directivity. The scatter plot in Figure 3.24 illustrates directivity and the corresponding K_{LOS}-factor for a link. It is obtained by calculating the overall experience directivity $D = D_{tx}D_{rx}$ from the measurements done by TU Wien which are illustrated in Figure 2.8, and the K_{LOS}-factor for a given link between pairs of ESLs. A clear correlation between both quantities can be observed.

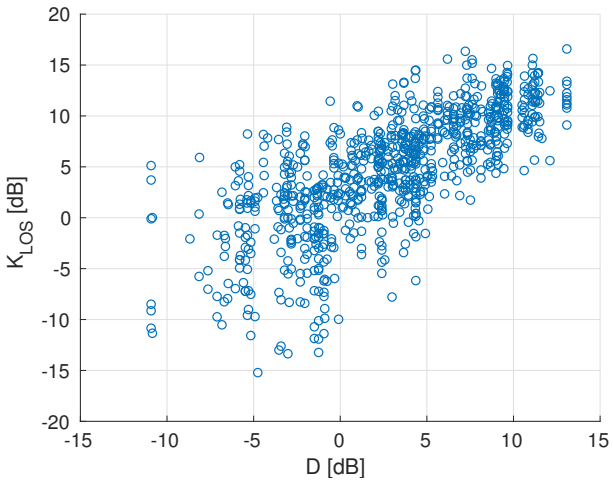

Figure 3.24: Distribution of the K_{LOS} factor in dependence of directivity

Delay Spread

The definition of the rms delay spread τ_{rms} is based on the averaged PDP. However, the evaluation presented here focuses on the instantaneous rms delay spread which is estimated from the instantaneous PDP defined in Equation (3.17). The instantaneous rms delay spread is given as

$$\tau_{\mathrm{rms}}\left(\mathbf{x}_{tx}, \mathbf{x}_{rx}\right) = \sqrt{\frac{\int_{-\infty}^{\infty} \tau^2 S\left(\mathbf{x}_{tx}, \mathbf{x}_{rx}, \tau\right) d\tau}{\int_{-\infty}^{\infty} S\left(\mathbf{x}_{tx}, \mathbf{x}_{rx}, \tau\right) d\tau} - \tau_{\mathrm{mean}}}. \tag{3.21}$$

The mean excess delay τ_{mean} is given as

$$\tau_{\text{mean}}\left(\mathbf{x}_{tx}, \mathbf{x}_{rx}\right) = \frac{\int_{-\infty}^{\infty} \tau S\left(\mathbf{x}_{tx}, \mathbf{x}_{rx}, \tau\right) d\tau}{\int_{-\infty}^{\infty} S\left(\mathbf{x}_{tx}, \mathbf{x}_{rx}, \tau\right) d\tau}. \tag{3.22}$$

The estimation of τ_{rms} is done similarly like the estimation of the K_{LOS}-factor. First, the noise floor is estimated and for the calculation of τ_{rms} is only the part of the PDP considered for which the PDP exceeds the noise floor significantly. The observed rms delay spreads for the different link conditions are illustrated in Figure 3.25. The *LOS* links show no significant difference, while a difference can be observed for the *NLOS* links. The difference is caused by the difference of the maximum received power as seen in the APDP in Figures 3.16 and 3.17.

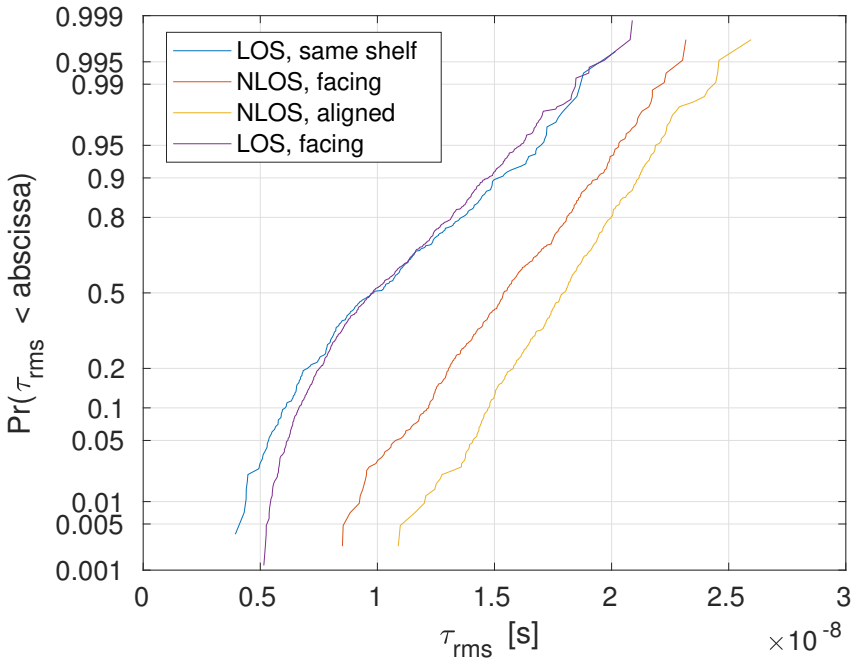

Figure 3.25: Empirical CDF of the estimated τ_{rms}

As mentioned in 3.1.2, the rms delay spread is inversely proportional to the coherence bandwidth. This is an important measure in terms of frequency diversity. The median values of the estimated rms delay spreads for the various links can be found to be in the range from 10-18 ns. According to Equation (3.12), the corresponding coherence bandwidths are in the range of 8 MHz to 15 MHz. The coherence bandwidth is an important measure to evaluate frequency diversity for mitigating small scale fading. From Appendix A.1, it can be seen that the maximum spacing between the eleven ESL channels is about 80 MHz. Moreover, up to four channels can be found to have a center frequency with a spacing less than the coherence bandwidth and therefore not all of the eleven channel can be used to for frequency diversity. Figures 3.27 and 3.26 show the spatial distribution of the rms delay spread for the setup described, as for the spatial distribution of the K_{LOS}-factor. The rms delay spread can be found to be almost inversely proportional to the K_{LOS}-factor presented in Figures 3.23 and 3.22.

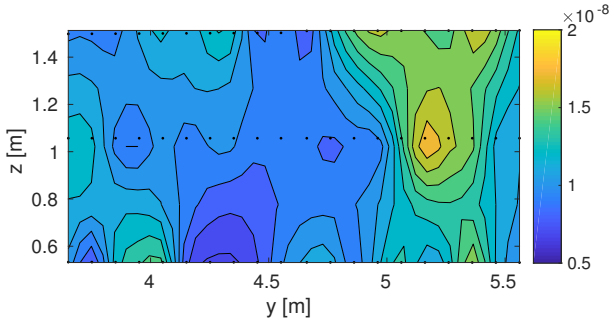

Figure 3.26: τ_{rms} distribution from the different Tx ESL positions on shelf S7 and S8 experienced by Rx ESL 7

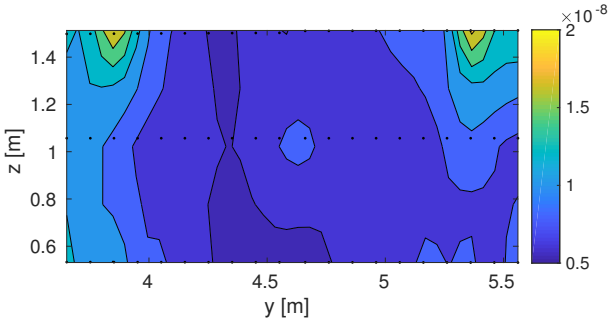

Figure 3.27: τ_{rms} distribution from the different Tx ESL positions on shelf S7 and S8 experienced by Rx ESL 5

Reverberation Time

The sound wave propagation and the electromagnetic wave propagation in rooms share some properties like the wavelength and hence are governed by same effects for in-room propagation [27]. Both, the sound pressure and the power delay are composed of specular and diffuse parts. Moreover, an exponential decay of the diffuse part can be observed in both cases. Thus, well established theory from acoustics is applied for electromagnetic propagation and leads to the theory of room electromagnetics. In room acoustics, reverberation is described by Sabine's or Eyring's equations. Both equations describe the reverberation time (decay time) of the exponential decay as a function of the room size V, the surface S and the effective absorption coefficient $\overline{a}$ [29]. The reverberation time given by Sabine's equation is

$$T_{Sab} = \frac{4V}{\overline{a}Sc}, \tag{3.23}$$

while Eyring's equation describe the reverberation as:

$$T_{Eyr} = \frac{-4V}{cS\ln(1-\overline{a})}. \tag{3.24}$$

Both models are validated by measurements for electromagnetics and show a good matching of the predicted and measured reverberation time. An important remark of the in-room electromagnetics is that the reverberation time is independent of the Tx-Rx separation [30].
In order to evaluate the distance dependency of the model, no correction of the propagation time is carried out like in Section 3.3.1. Figure 3.28 illustrates the APDP of the different links with the indicated constant reverberation time. The reverberation time is estimated in the log domain and hence is done by least squares fitting of a linear equation of the form $\mathbb{E}\{|h_{diff}(\tau)|^2\} = P_{diff} - \frac{1}{T}\tau$ to the data, where P_{diff} is a constant power at $\tau = 0$ and T is the reverberation time. The fitting was done between $\tau_{\text{start}} = 35$ ns and $\tau_{\text{end}} = 120$ ns to suppress the influence of the dominant component at the beginning and the noise floor at the end of the tail. The decay time T and the constant P_{diff} were estimated for each link condition independently. Table 3.2 lists the estimated parameters. It can be seen that the decay constant is independent of the link and just P_{diff} varies in the range of 4 dB.

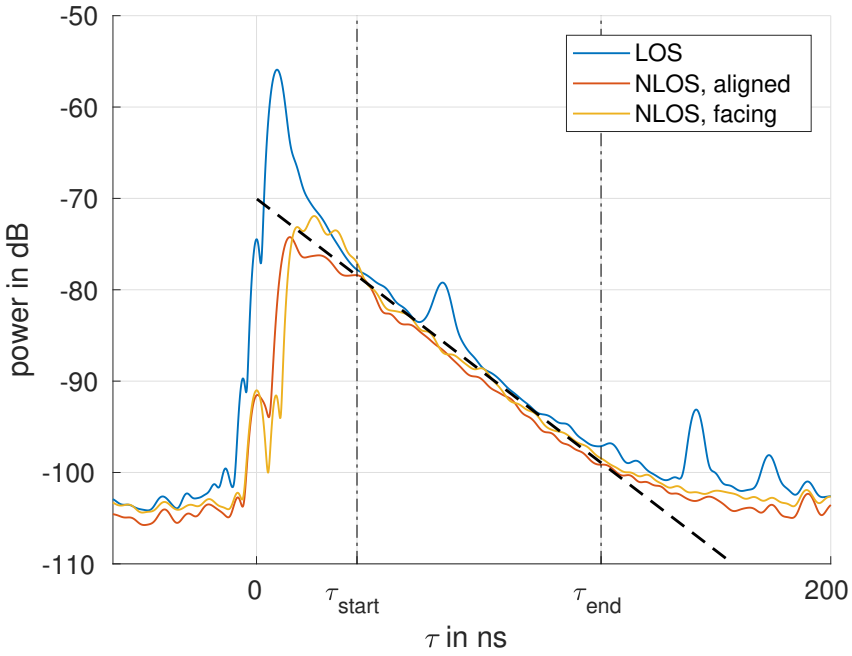

Figure 3.28: Estimation of the reverberation time

Scenario	constant k	T
LOS, facing	-68.26 dB	17.52 ns
LOS, same shelf	-67.34 dB	17.41 ns
NLOS, aligned	-71.07 dB	18.12 ns
NLOS, facing	-70.75 dB	18.5 ns

Table 3.2: Estimated parameters or the reverberation model

3.4 Measurements with Electronic Shelf Labels

The measurement campaign with the ESLs verifies the measurements with the channel sounder. Figure 3.29 illustrates the mean RSSI values between all possible links of pairs of ESLs. The figure visualizes again that only two out of the five link conditions can be distinguished, namely LOS and NLOS link condition. Subdivision of the measured RSSI values is not possible. The effect of AGC freezing is visible by the white spots for which no measurements were available due to saturation of the RX.

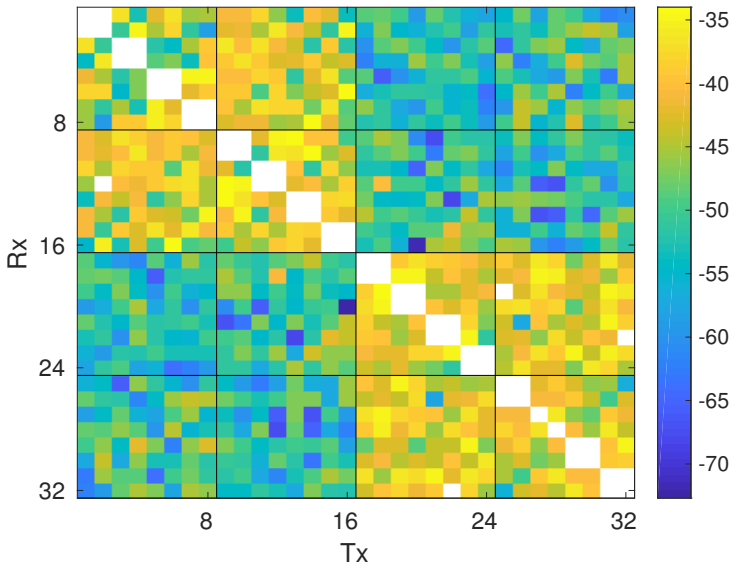

Figure 3.29: RSSI values in dBm for different links

Although the upper range of RSSI values is limited due to AGC freeze, links, for which no RSSI value is reported, do provide important information. There are three important remarks about the observation illustrated in Figure 3.29. First, non-connected ESLs are not only on the same shelf. Instances of non-connectivity can also be found between Rx ESL 2 and Tx ESL 12 as illustrated in Figure 3.30 or between ESL 22 and 32 like in Figure 3.31. While the non-connectivity between the pair ESL 22 and ESL 32 is reciprocal, the non-connectivity of ESL2 and ESL12 is observed only for one direction. The reason for this circumstance is found in the tolerance of the configured transmit power as well as the tolerance in the receiver amplifier. On the other hand, the non-connectivity between ESL 2 and ESL 12 is reciprocal meaning that both receivers are in saturation. This observation is equivalent to the observations made in the measurement campaign with the channel sounder. ESLs show a better connection for diagonal links than for links with an azimuth angle of about 0°

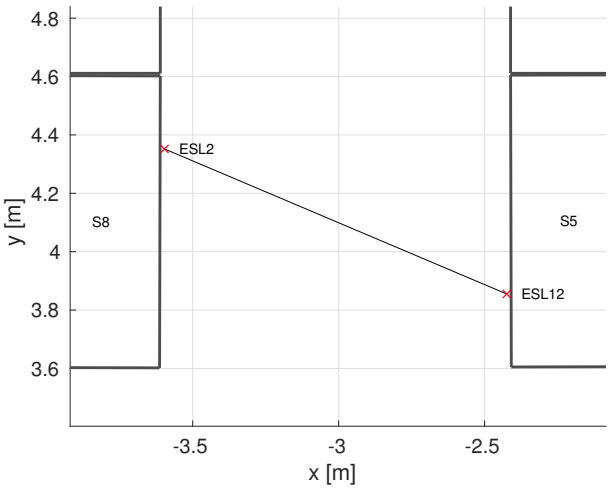

Figure 3.30: Example 1 of a strong link between opposite shelves

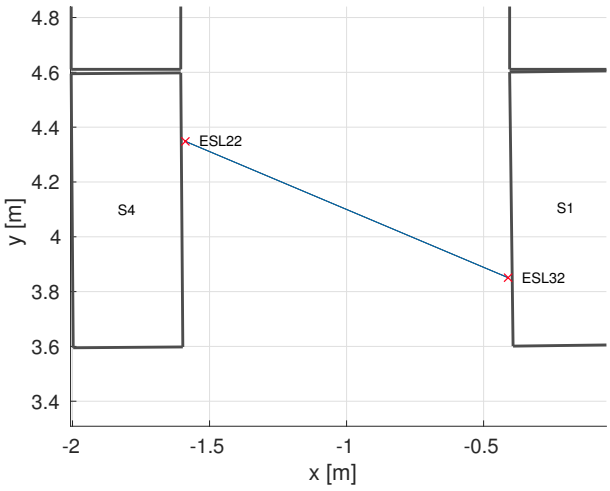

Figure 3.31: Example 2 of a strong link between opposite shelves

The second remark concerns the non-connectivity between ESLs on the same shelf. ESLs on the same shelf do not have a connection as long as they are placed on the same shelf level. Only between ESL 27 and ESL 28, a connection was established. However, links can be established

between ESLs on shelves which are placed next to each other. Figure 3.32 depicts this situation. A connection between ESL1 and ESL2 is not possible while it is for ESL2 and ESL3 although the spacing is almost the same. This circumstances can be observed for all ESLs. The reason for this effect is given by coupling over the shelf level which are made of metal. ESL 1 and ESL 2 are placed on the same shelf level while ESL 2 and ESL3 are place on different shelves and therefore no coupling effects can be experienced.

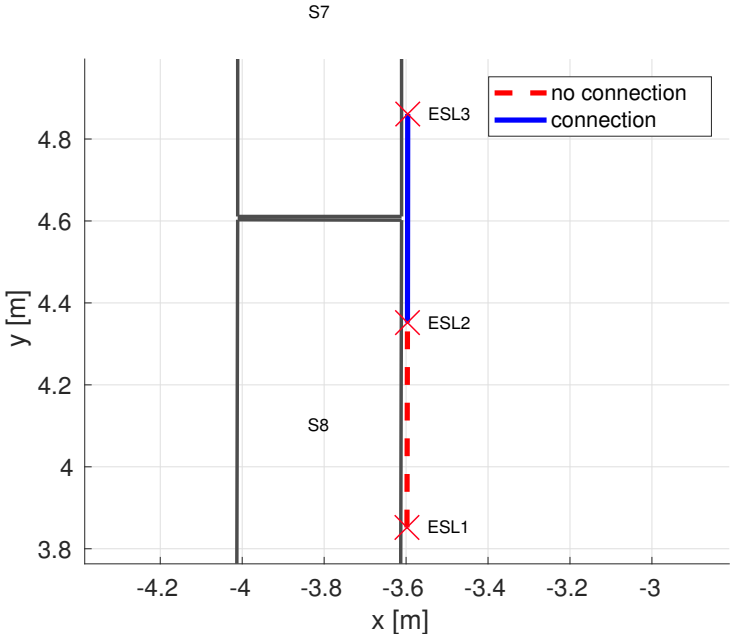

Figure 3.32: Connectivity between ESLs

The last remark addresses the same situation between ESLs on the same shelf but on different levels. For instance ESL1 and ESL5 are placed on shelf 8 at position 1 at level 2 and 3, respectively. Between these two ESLs, a link was possible while no link was possible between ESL1 and ESL2 since they were placed on the same level. The reason can be found again in the coupling on of ESLs placed on the same shelf level. To summarize, an influence of the shelf itself can be observed due to coupling over shelf levels.

Statistics of RSSI values

In order to compare the statistics of the RSSI values with the estimated path losses in Section 3.2.1 the negative RSSI values are considered since they are related to the path loss by a constant offset given by the transmit power. The empirical CDF of the measured RSSI is illustrated in Figure 3.33 values It can be seen that the negative RSSI values cover almost the same range as the estimated path loss values from the measurement campaign with the channel sounder, except the low path loss values observed for the same-shelf measurement which have been lost due to the saturation effects described before. Another fact which validates the measurement of the channel sounder is that the measurements fall into two groups, namely LOS and NLOS groups.

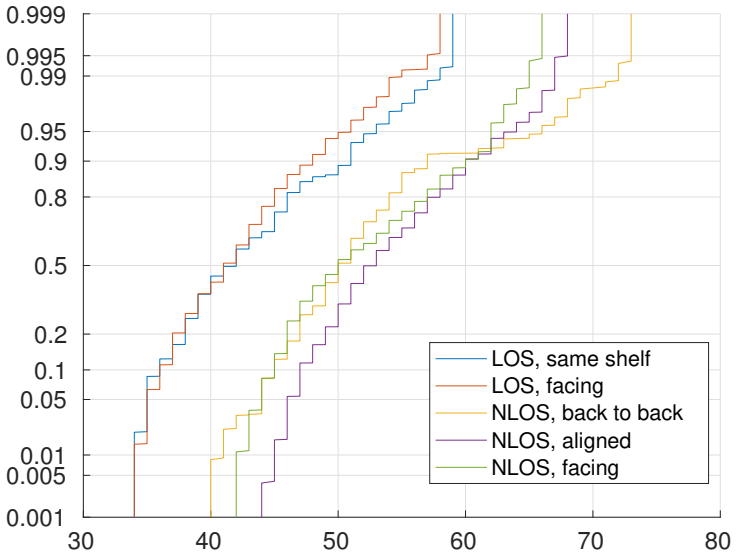

Figure 3.33: Empirical CDF of the negative RSSI values in dBm

Stability of RSSI values

The stability of the RSSI values is evaluated in terms of the standard deviation of the observed RSSI values between any pair of ESLs. The measurement setup was remote controlled by an operator who was not present in the room during the measurement. Thus, a static environment was given over the whole measurement time. Figure 3.34 presents the estimated standard deviation of the RSSI values. A good stability of the RSSI values is observed. The highest standard deviation can be found for links with a low RSSI value. For instance, the link between ESL 16 and ESL 20 has a standard deviation of 0.85 dB while the mean is -72.69 dB. A close look at the measured RSSI values shows that they vary in the range from -71 to -73 dB. Another instance of this behaviour can be found for ESL 12 and ESL 28. In both cases is the variation of the RSSI values reciprocal.

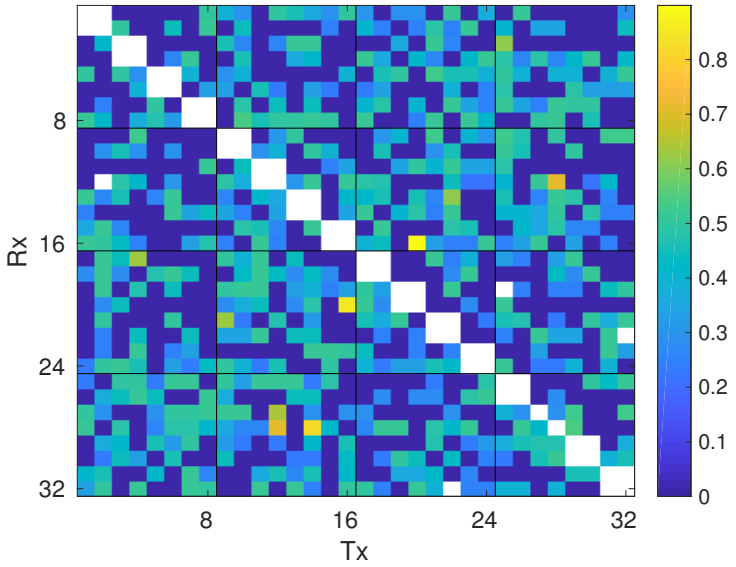

Figure 3.34: Standard deviation of RSSI values in dB

Reciprocity of RSSI Values

Beside the stability, the reciprocity of the RSSI values is of interest. Figure 3.35 illustrates the difference of the mean RSSI values which is obtained by subtracting the transposed matrix of mean values from the matrix with the mean values which is illustrated in Figure 3.29. The RSSI values show a good reciprocity since the majority of the differences are around 0 dB. The quantization step size of the measured RSSI values is 1dBm and a fluctuation of the RSSI value around $\pm$ 0.5 dB are expectable. Hardware induced mismatch of the RSSI values can be seen for instance for ESL 25 (marked by the red rectangular). ESL25 measures lower RSSI values from all other ELSs than vice versa.

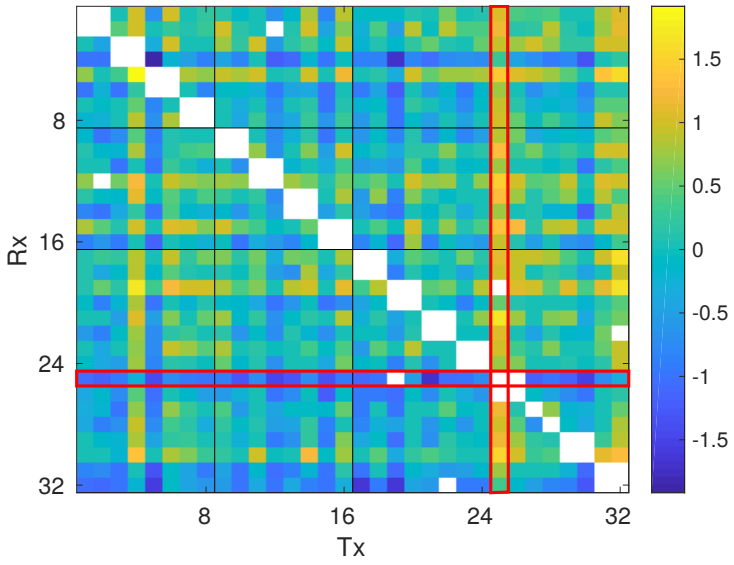

Figure 3.35: Differences between reported RSSI values in dB

Influence of Small Scale Fading

The 32 ESLs can be divided into two groups of 16 ESLs which were placed in the two different corridors. Within each corridor, the ESL are placed at the same position. As a consequence, all ESLs within one group have the same relative distances to all other ESLs within a group. Deviations in the range of cm were not avoidable due to manufacturing tolerances of the shelves. However, this setup makes it possible to evaluate the influence of small scale fading. Therefore, the differences between the ESLs of one group and the corresponding ESL of the other group is calculated. Figure 3.36 illustrates the differences of the corresponding RSSI values. The maximum difference of the mean values is 17.15 dB while the standard deviation of the differences is 6 dB.

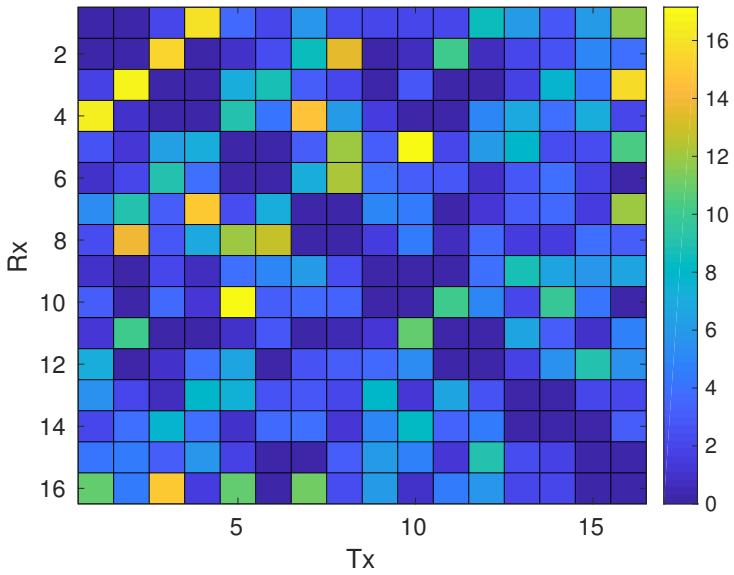

Figure 3.36: Deviation of RSSI in dB due to small scale fading in dB

3.5 Proposed channel model

The need of a channel model is two-fold. First by it should help in deriving localization algorithms and second by it should be utilized for simulation purposes in order to evaluate the performances of localization algorithms. Based on the observations made in the measurement campaign, it is proposed to model the channel by a deterministic LOS component and diffuse multipath.

$$h\left(\mathbf{x}_{tx}, \mathbf{x}_{rx}, \tau\right) = \alpha\left(\mathbf{x}_{tx}, \mathbf{x}_{rx}\right) \delta\left(\tau - \tau_{LOS}\right) + \nu\left(\mathbf{x}_{tx}, \mathbf{x}_{rx}, \tau\right), \tag{3.25}$$

where $\alpha\left(\mathbf{x}_{tx}, \mathbf{x}_{rx}\right)$ is the complex valued amplitude of the LOS component, $\delta(\cdot)$ denotes the Dirac delta and $\nu\left(\mathbf{x}_{tx}, \mathbf{x}_{rx}, \tau\right)$ is the dense multipath described by a random process. τ_{LOS} describes the propagation time of the signal between a Tx and Rx and is given as:

$$\tau_{LOS} = \frac{1}{c}\|\mathbf{x}_{tx} - \mathbf{x}_{rx}\|, \tag{3.26}$$

where $\|\mathbf{x}_{tx} - \mathbf{x}_{rx}\|$ is the Euclidean distance between the transmitter and receiver positions $\mathbf{x}_{tx}$ and $\mathbf{x}_{rx}$ and c is the speed of light.

The statistics of the channel is derived from the APDPs obtained in Section 3.3.1. For LOS links, a dominant component can be identified while for NLOS links this component is missing. Independent of the LOS component, an exponentially decaying diffuse multipath is present, which decays with the same decay time independently of the link.

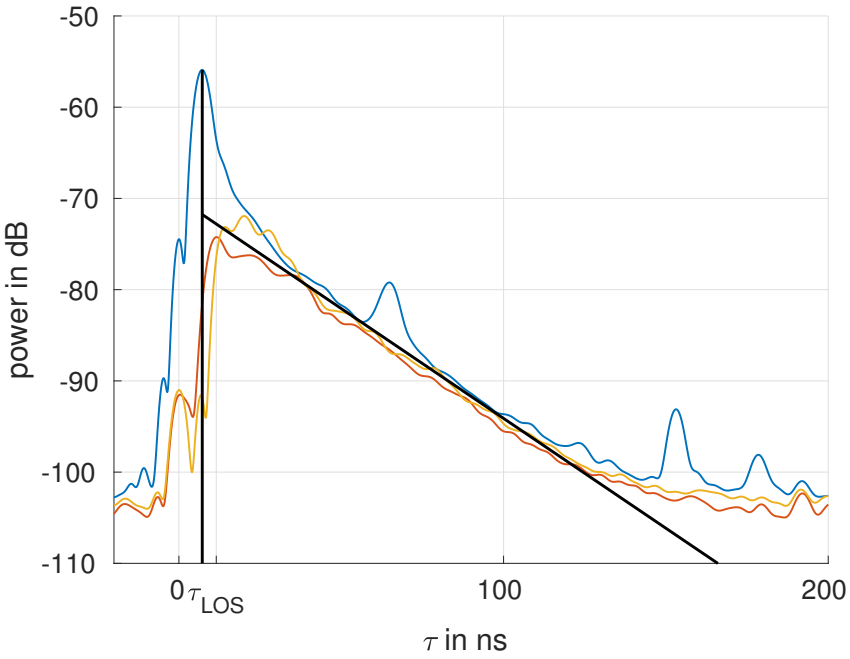

Figure 3.37: APDPs with indicated model

The PDP is composed of two parts:

$$S\left(\mathbf{x}_{tx}, \mathbf{x}_{rx}, \tau\right) = S_{LOS}\left(\mathbf{x}_{tx}, \mathbf{x}_{rx}, \tau\right) + S_{\nu}\left(\mathbf{x}_{tx}, \mathbf{x}_{rx}, \tau\right), \tag{3.27}$$

where $S_{LOS}\left(\mathbf{x}_{tx}, \mathbf{x}_{rx}, \tau\right)$ is the PDP of the LOS (direct) part and $S_{\nu}\left(\mathbf{x}_{tx}, \mathbf{x}_{rx}, \tau\right)$ the PDP of the diffuse multipath components. The LOS part is a deterministic function given by Friis equation:

$$S_{LOS}\left(\mathbf{x}_{tx}, \mathbf{x}_{rx}, \tau\right) = \begin{cases} \frac{D_{tx}(\mathbf{x}_{tx}, \mathbf{x}_{rx}) D_{rx}(\mathbf{x}_{tx}, \mathbf{x}_{rx}) \lambda^2}{(4\pi)^2 \|\mathbf{x}_{tx} - \mathbf{x}_{rx}\|^2 L} \cdot \delta\left(\tau - \tau_{LOS}\right) & \text{if LOS is unobstructed} \\ 0 & \text{else} \end{cases}, \tag{3.28}$$

where $D_{tx}\left(\mathbf{x}_{tx}, \mathbf{x}_{rx}\right)$ and $D_{rx}\left(\mathbf{x}_{tx}, \mathbf{x}_{rx}\right)$ are the directivities of the transmitter and receiver antenna respectively. The system loss L in the denominator addresses system losses which cannot be captured by the model like antenna losses due to mismatching or coupling losses with the shelf itself. The system loss was estimated by minimizing the error between the predicted power of the LOS component and the measured received power. A minimum error was found for a system loss L of 2.3 dB. Based on the separation distance, the propagation time can be calculated as follows: The constant decay time of the diffuse multipath is modelled as:

$$S_{\nu}\left(\mathbf{x}_{tx}, \mathbf{x}_{rx}, \tau\right) = S_{\nu,0} \exp\left(-\frac{\tau}{T}\right) u(\tau - \tau_{LOS}), \tag{3.29}$$

with $u(\cdot)$ beeing the unit step function which models the onset of the dense multipath power. This definition follows the model given in [31]. The diffuse gain is characterized by the parameter $S_{\nu,0}$ and the decay time constant T. Both parameters have been estimated in Sec 3.3.1.

Based on the model for the APDP, a model can be derived for the diffuse multipath part of $\nu(\tau)$ the channel in Equation (3.25)

$$S_{\nu}\left(\mathbf{x}_{tx}, \mathbf{x}_{rx}, \tau\right) = \mathbb{E}\{|\nu\left(\mathbf{x}_{tx}, \mathbf{x}_{rx}, \tau\right)|^2\}. \tag{3.30}$$

Model Implementation for Simulation

The version of the CIR is implemented in two steps. In the first step, the deterministic component of the signal is computed. The absolute value of the complex amplitude reads according the Equation (3.28):

$$|\alpha| = \sqrt{\frac{D_{tx}\left(\mathbf{x}_{tx}, \mathbf{x}_{rx}\right) D_{rx}\left(\mathbf{x}_{tx}, \mathbf{x}_{rx}\right) \lambda^2}{\left(4\pi\right)^2 \left\|\mathbf{x}_{tx} - \mathbf{x}_{rx}\right\|^2 L}}. \tag{3.31}$$

The phase of the complex amplitude is computed from the propagation time and is given as:

$$\arg\left(\alpha\right) = 2\pi f_c \tau_{LOS}. \tag{3.32}$$

α is assigned to the closest sample $\delta\left(\tau - \tau_{LOS}\right)$. In the second step is $S_\nu\left(\mathbf{x}_{tx}, \mathbf{x}_{rx}, \tau\right)$ computed which describes the shape of the diffuse part. A single realization of the diffuse multipath is obtained by generating samples of the a zero-mean complex circular symmetric normal distribution with statistics $\mathbb{E}\{\nu(\tau_i)\nu(\tau_j)\} = S_\nu \delta(i-j)$. Finally, the resulting CIR is convolved with the desired pulse.

3.5.1 Validation of the Model

The model and its implementation are validated by comparing both, the wideband and narrowband results against the real measurements.

Wideband

The model shows a good match for the LOS component for the two *LOS* links. The diffuse part is also modelled accurately but it does not follow exactly the exponentially decay. A power law or double exponential shape might show better fitting.

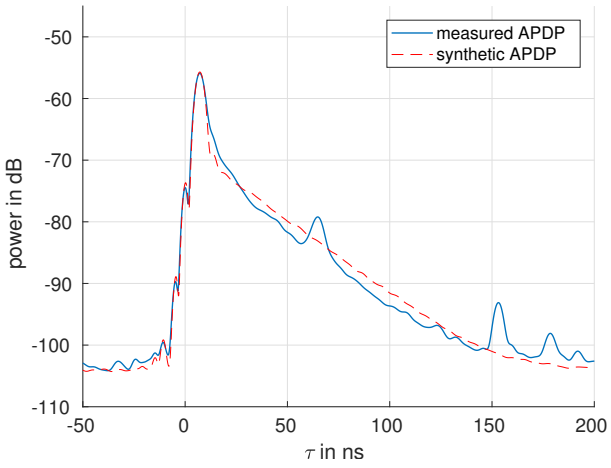

Figure 3.38: Comparison between measured and synthetic APDP for the LOS, facing *link*

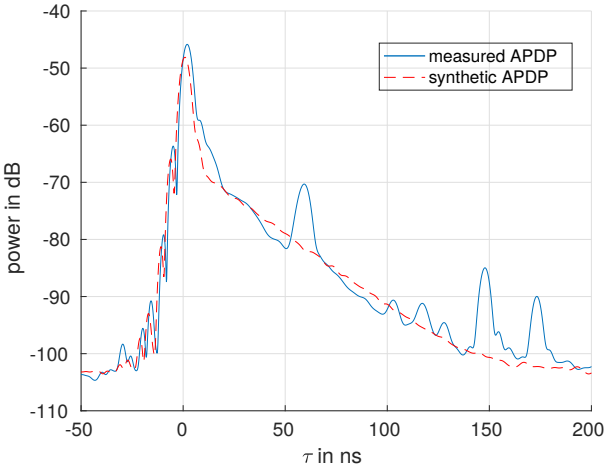

Figure 3.39: Comparison between measured and synthetic APDP for the LOS, same shelf *link*

On the other hand, the exponential decay models the shape of the diffuse part with an high accuracy and only small deviation can be seen.

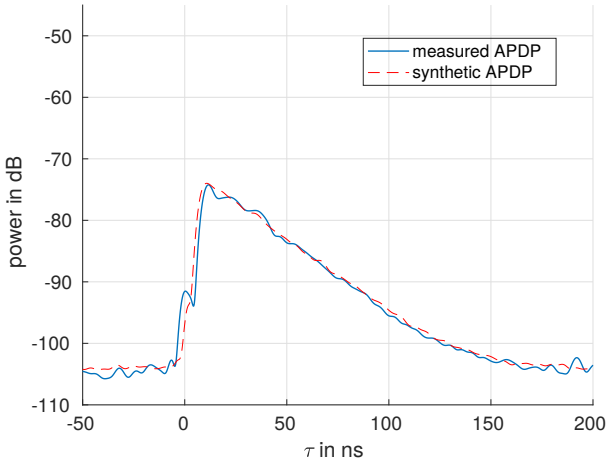

Figure 3.40: Comparison between measured and synthetic APDP for the NLOS, aligned *link*

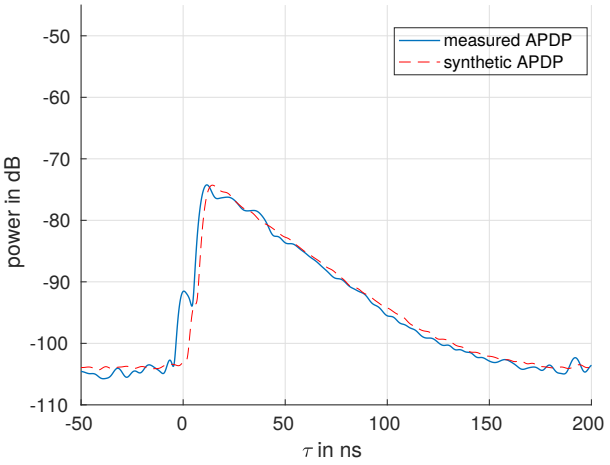

Figure 3.41: Comparison between measured and synthetic APDP for the NLOS, facing *link*

Narrowband

In order to compare the narrowband results of the measurement campaign with the channel sounder are the synthetic generated CIRs post-processed like the measured CIRs. Therefore pulse shaping of the CIRs was performed with a raised cosine pulse with the same parameter as presented in Section 3.2.1. The synthetic narrowband data show a good match for the two evaluated *NLOS* links over the entire range, see Figures 3.44 and 3.43

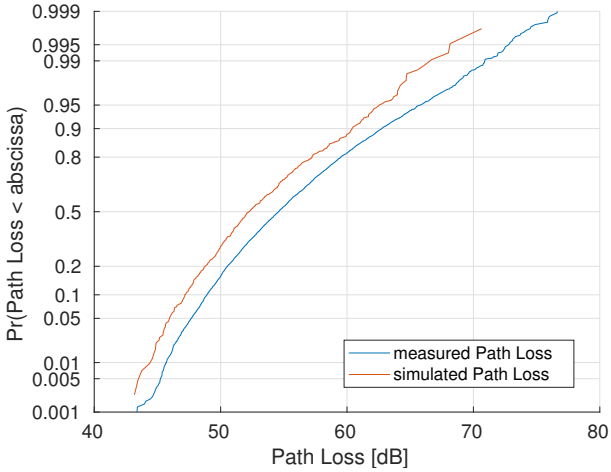

Figure 3.42: Comparison between the synthetic and measured path losses of the NLOS, aligned *links*

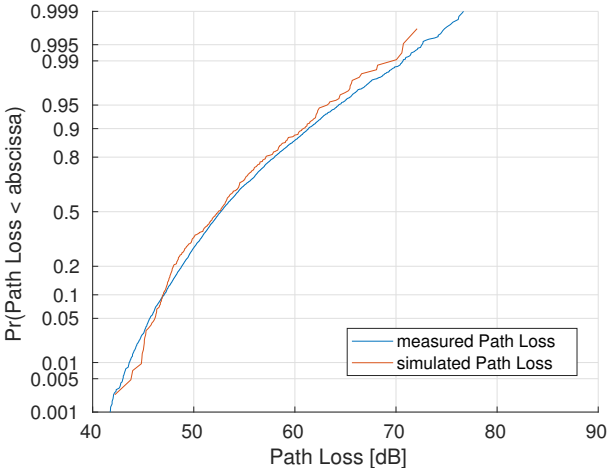

Figure 3.43: Comparison between the synthetic and measured path losses of the NLOS, facing *links*

An offset can be observed between the synthetic modelled and measured path losses for the *LOS, facing*, see Figure 3.42. This offset is against the expectations since the additional strong components are not modelled. The comparison of the *LOS, same shelf* link in Figure 3.45 shows for the lower range a good match of the path loss while a divergence between the model and measured data can be seen for the upper range of path loss values.

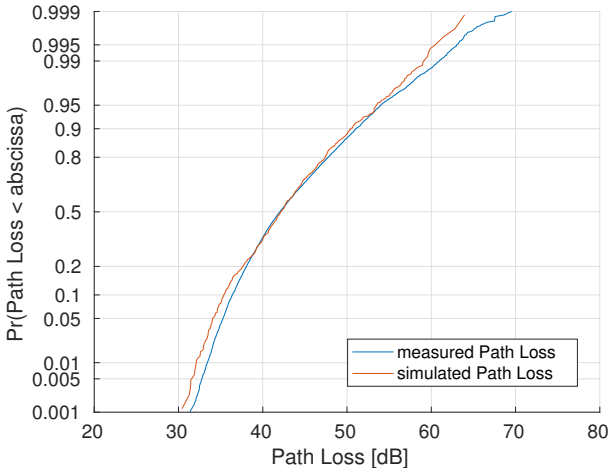

Figure 3.44: Comparison between the synthetic and measured path losses of the LOS, facing *links*

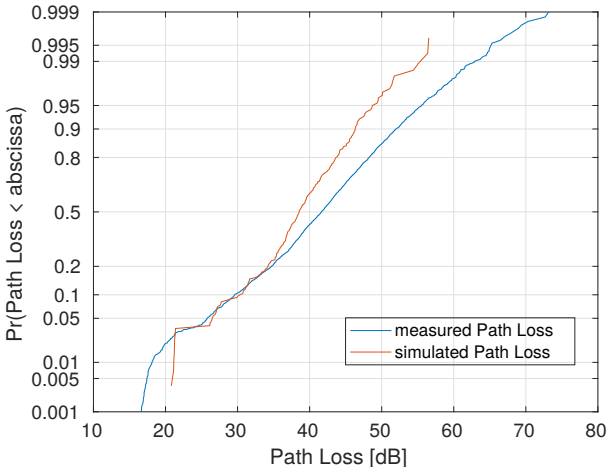

Figure 3.45: Comparison between the synthetic and measured path losses of the LOS, same shelf *links*

4 Localization Algorithm

The results of the measurement campaign provide important insights for localization algorithms. Localization algorithms discussed in Section 1.2 exhibit position errors in the order of a meter up to tens of meter in indoor environments. However, the area of interest is in the same order and therefore, such algorithms are not suitable for the desired localization task. Moreover, position algorithms typically estimate the position within a given search space which is usually a 2D area where each position is a possible solution. On the other hand, the position of ESLs are aligned with shelves or racks and therefore are not freely placed within the area of interest. This restriction limits the usage of localization algorithms based on a gradient based optimization of a cost function in order to find the position estimate.
Based on the observation of the measurement campaign, it can be seen that the assigning of a shelf to a Tx ESL is a challenging task. Figures 4.1 and 4.2 emphasize this circumstance. The range of path loss values from 40 dB upwards can be found for all link conditions. However, there are about 20% of unique path loss values for links on the same shelve. 50% of the path loss values of the LOS can be seen to be unique for ESLs placed in the same corridor. Figure 4.2 illustrates also the limited usage of RSSI values for ranging since they carry less distance information for such a layout. A clear distance path loss correlation can only be seen for distances up to 0.5 m.

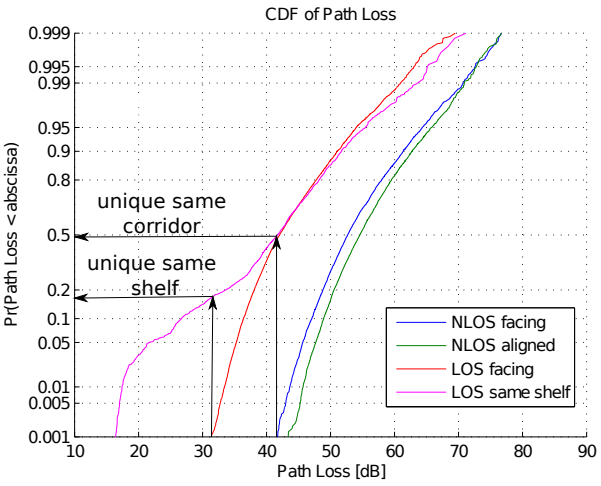

Figure 4.1: Path Loss distribution for LOS and NLOS links

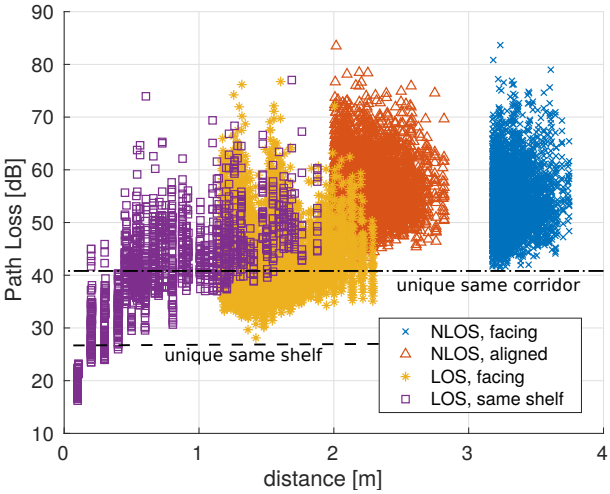

Figure 4.2: Path Loss vs. distance for LOS and NLOS links

Localization can be done in a two step approach. In the first step, it is desirable to detect the corridor or even more preferable the correct shelf. Once the correct corridor/shelf for an ESL is detected, cooperative localization algorithms could be utilized to determine the position on a shelf.

4.1 Shelf Detection

The task of detecting the correct corridor or shelf can be described in the following way: Given a set of ESLs with known positions, so called anchors, what is the most likely shelf of an ESL given the RSSI values between the ESL and the anchors? A possible solution to this problem is to utilize the probability distribution of the given links. In case that the statistics are known, a maximum likelihood (ML) approach can be applied for the decision making process. The posterior probability can be defined as

$$P\left(x|p\right) = \frac{f\left(p|\, L(x)\right) P(x)}{\sum_{n=1}^{4} f\left(p|\, L(x_n)\right) P(x_n)}, \tag{4.1}$$

with $x \in \{\text{'S1/S2'}; \text{'S3/S4'}; \text{'S5/S6'}; \text{'S7/S8'}\}$ being the hypothetical shelf postion and p being the measured power. $L(x)$ is a functional map which maps from the hypothetical shelf position x to the corresponding pdf of the power p based on the link condition between the anchor and hypothetical shelf position x. $P(x)$ is the prior distribution of the shelf position. In the following, $P(x)$ will be assumed to be uniformly distributed and therefore does not provide any information. In case of several measurements, Equation (4.1) can be extended to:

$$P(x|\mathbf{p}) = \frac{\prod_{n=1}^{N} f(p_n|L_n(x))P(x)}{\sum_{i=1}^{4}\prod_{n=1}^{N} f(p_i|L_i(x))P(x_n)} \tag{4.2}$$

where $\mathbf{p} = [p_1, p_2, \ldots, p_N]^T$ is a vector holding all the measured power values. Knowledge about the PDFs $f\left(p|\, L(x)\right)$ is required in order to utilize an ML estimator. It was shown in Section 3.2.1 that the amplitude for the *LOS, facing* and the two *NLOS* links were Rayleigh distributed and therefore, the received power is exponentially distributed. However, the received power for the *LOS, same shelf* cannot be described by an exponential distribution. The exponential distribution is described by the a single parameter λ. The corresponding λ-values for the different link conditions were estimated from the histograms and are presented in Table 4.1. The *NLOS, back to back* was not evaluated in detail and hence sufficient measurements are not available in order to estimate the parameter of the distribution. However, it can be assumed that it shares the same distribution like the *NLOS, aligned* distribution and therefore, this parameter will be used in further experiments.

Link Condition	λ
LOS, facing	$1.05 \cdot 10^4$
NLOS, aligned	$1.85 \cdot 10^5$
NLOS, back to back	
NLOS, facing	$1.12 \cdot 10^5$

Table 4.1: Parameters of the different link conditions

A more complicated situation is given for the *LOS, same shelf* link since it cannot be described by an exponential distribution with one parameter. The upper part of the CDF follows an exponential distribution. For the sake of simplicity, a mixture of two exponential distributions will be used for the experiment. The mixture distribution can be described by:

$$f(p) = \beta\lambda_1 \mathrm{e}^{\lambda_1 p} + (1-\beta)\lambda_2 \mathrm{e}^{\lambda_2 p} \tag{4.3}$$

where β is a weight between the two distributions. The parameters of the mixture distribution are given in Table 4.2.

Parameter	Value
β	0.85
λ_1	$1.6 \cdot 10^4$
λ_2	$2 \cdot 10^2$

Table 4.2: Parameters of the mixture distribution

Figure 4.3 provides a comparison of the CDF of the path loss of the measured data and the mixture distribution.

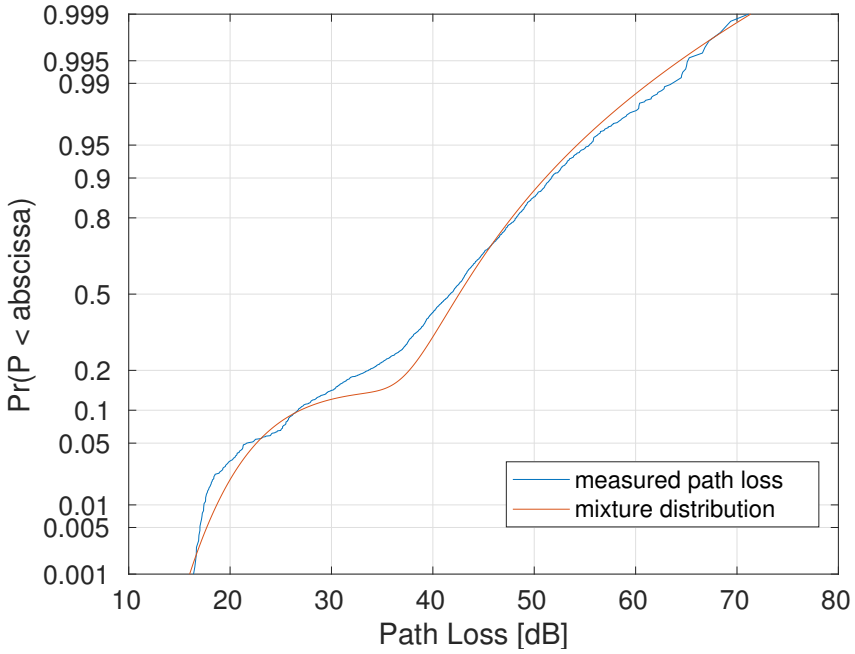

Figure 4.3: CDF of the mixture of two exponential distribution

4.1.1 Evaluation

The results of the channel sounder measurement campaign were used for the evaluation of the introduced algorithm. More specifically, the results from the evaluation of the *LOS, facing*, *NLOS, aligned* and *NLOS, facing* link conditions were used. The link conditions were evaluated at seven Rx ESL positions for the *NLOS, aligned* and *NLOS, facing* link conditions and at 14 Rx ESL positions for the *LOS, facing* link conditions. The Rx ESLs are considered in the following as anchors. Up to seven anchors per link condition were evaluated. The posterior probability was evaluated for all 60 measured Tx positions on shelves S7 and S8 which forms the ground truth. Figure 4.4 illustrates the probability of the hypothesis X = 'S7/S8' for all 60 Tx positions. The position of the anchors on the shelves was chosen randomly. Beside the median are the upper and the lower quartiles illustrated. It can be seen that the median of all probabilities increases from 0.5 for one anchor up to almost 0.9 for seven anchors. The lower quartile does not increase in the same rate and can be found to be 0.55 for seven anchors. This indicates that there is still a high number of outliers which causes a wrong decision. Figure 4.5 illustrates the evolution of the probability of a single Tx ESL for the hypothesis X = 'S7/S8' for different configurations of anchors positions. An increase form 0.5 to 0.8 can be seen as the number of anchors increase. Also the quartiles increase at the same rate and can be found to be in a range of ± 0.05 for seven anchors indicating that the single probabilities are not spread

over a wide range.

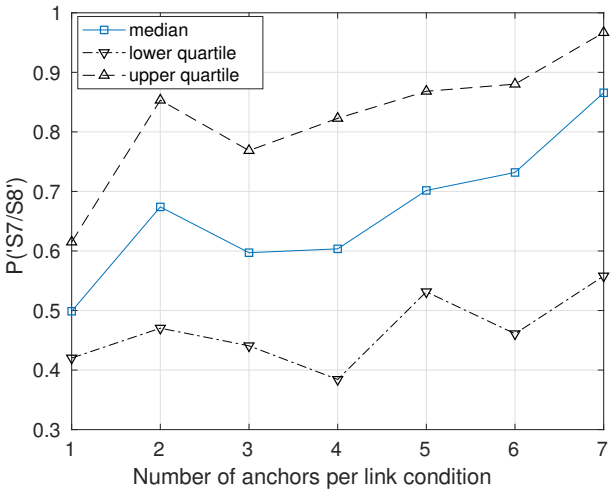

Figure 4.4: P('S7/S8') for all Tx ESLs

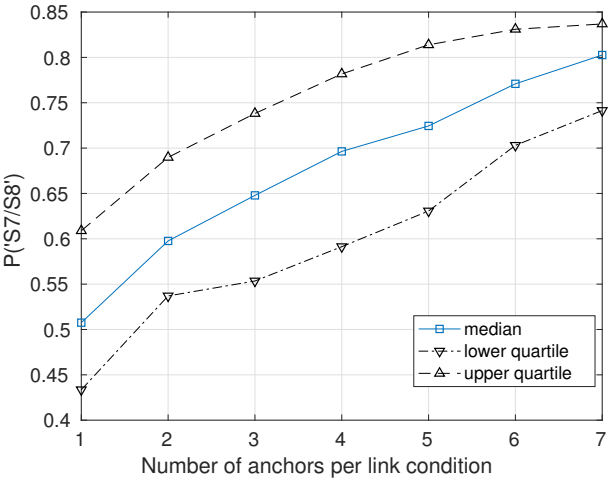

Figure 4.5: P('S7/S8') for one Tx ESL and different configurations of anchors positions

Figure 4.6 illustrates the resulting probability mass function (PMF) of the decision for a hypothesis based on the posterior probability (4.2). The measured data sets have been analyzed for that purpose, evaluating all Tx positions on shelves S7/S8 w.r.t. different Rx configurations on the other shelves, i.e. on S1-S6. Same-shelf measurements have been excluded because they were not available in this data set. It can be seen that already one anchor ESL per link condition can detect the correct corridor with a high accuracy but still some decisions for shelves S1/S2 and S3/S4 can be observed. Between the hypotheses S5/S6 and S7/S8, a decision is more difficult. This circumstance is given due to the fact that the *NLOS* links have almost the same PDF and thus does not provide more information. However, already two anchors per link condition are sufficient to decide for the correct corridor. After considering five anchors per shelf pair, no significant improvement can be observed.

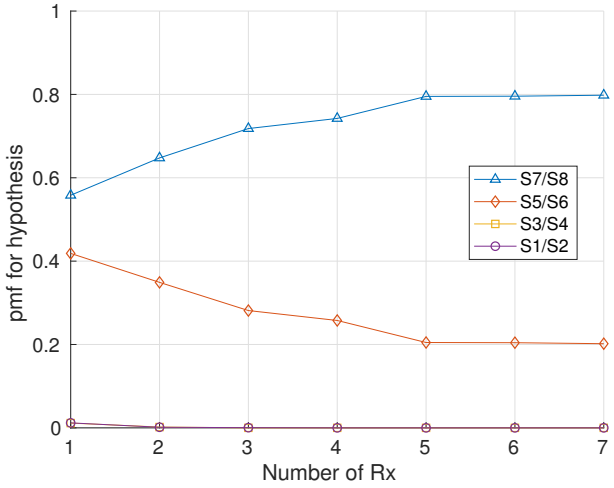

Figure 4.6: PMF for the hypothesis for a different number of Rx

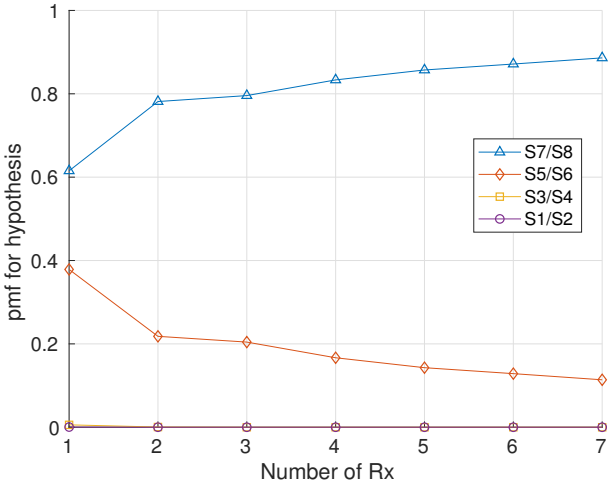

Figure 4.7: PMF for the hypothesis by utilizing frequency diversity for a different number of Rx

An improvement of the algorithm can be achieved by utilizing narrowband measurements obtained at different channels. For the decision making, the probabilities of the single measurements were normalized and combined in order to make a soft decision. It can be seen that averaging improves the probability for the correct shelf/corridor, especially for a low number of

anchors. Already one anchor per shelf pair is sufficient to decide for the correct corridor. Two anchors show almost the same result as for seven ESLs do for a single measurement.
Two important remarks can be made about the experiment. First, measurements between ESLs on the same shelf are not included. Just the corresponding PDF was used in the hypothesis testing. A further improvement of the detection accuracy could be expected if measurements between ESLs on the same shelf are included, especially for closely-spaced ESLs. Second, the evaluation was only performed for anchors which were placed in the positive x direction from shelf pair S7/S8. If measurements for the Tx ESLs in the negative x direction would be available a further increase of the detection probability could be expected.

5 Conclusion and Outlook

5.1 Conclusion

RSS-based localization is a challenging task, especially if sub-meter accuracy is required. Section 2.2.1 illustrated the influence of the environment on the directivity of the ESL. The directivity of the antenna changes by the way of mounting onto a shelf. Several different ways are possible and different types of shelves can be found which makes direct application of the directivity difficult. Chapter 3 evaluated the channel for the narrowband and wideband cases. The antenna is considered as a part of the channel which can be found to have great influence on the overall channel characteristic especially for LOS links. A distance dependency of the path loss could only be observed for closely spaced ESLs up to 0.5 m. Moreover, the path losses can only be divided into two groups, namely LOS and NLOS. The wideband results reflect again the influence of the antenna pattern for LOS links. For NLOS links only dense multipath can be observed. The diffuse multipath was shown to follow an exponentially decaying PDP with constant decay time, independent of the observed link condition. In Section 3.5, a channel model was introduced and its accuracy verified against the measured data which shows a good match. Chapter 4 focused on localization algorithms based on the evaluation of the channel measurements. A two-step approach is proposed, where in the first step the corresponding shelf is estimated based on the statistics of the received power. It was shown that the shelf/corridor can be detected with high probability which can be improved by utilizing frequency diversity. The second step aims to determine the position of an ESL on a shelf which is not part of this thesis.

5.2 Outlook

A promising approach for reaching the aim of sub-meter accuracy are probabilistic models such as factor graphs which are subject of research in wireless sensor networks (WSN) [33]. The ESL localization task can be formulated in a graphical model where ESLs are vertices of a graph and connections between ESLs are given by the edges of the graph. The position of an ESL can be formulated as a probability distribution of positions which is conditioned on the position of the other ESLs to which it is connect. This conditional probability can be factorized and makes factor graphs a suitable tool for the localization task. Sum-product algorithms and belief propagation algorithms [34] have been successfully applied to the localization task in WSNs. The challenge for such algorithms will be to formulate the desired localization task and find accurate probabilistic models.

A ESL

A.1 ESL Channels

ESL channel	Frequency / MHz
0	2404.198486
1	2410.147034
2	2422.044128
3	2424.843445
4	2441.989258
5	2449.337463
6	2461.934387
7	2469.632507
8	2474.531311
9	2476.980713
10	2479.430115

Table A.1: Center frequencies of the ESL channels, Source: [20]

ses imagotag

PRODUCT / ELECTRONIC SHELF LABELS

G1 2.6 BWR NFC

TECHNICAL DETAILS

Product Code	R26N01
Dimensions (mm)	83.6 x 42.5 x 16.3
Weight	45 g
Standard cover frame	White
Display technology	Full graphic E-ink display
Active display area (mm)	60.1 x 30.7
Resolution (pixels)	296 x 152
Pixel density	125 dpi
Pixel Colors	Black/white/red
Viewing angle	Nearly 180°
Usable pages	4*
Label updates/hour/AP	4500 (2600 in FCC/IC mode)
Operating temperature	10° C to 40° C
Battery lifetime (room temperature)	5 years (2 updates/day)*
Battery	3V lithium manganese dioxide button cell battery pack, replaceable by customer (available as a spare part)*
Encryption	128-bit AES with secure key exchange
Water resistance	Yes
Compliance	CE, ROHS, FCC, IC
Packaging unit	80 label/box
NFC	Yes, operating frequency: 13.56 MHz
ESL operating frequency	2.400-2.480 GHz, maximum EIRP ≤ 10 mW
Wireless firmware update	Yes

*for details see product specification

EXEMPLARY PICTURE

TECHNICAL DRAWINGS

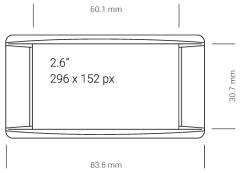

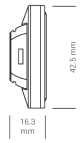

© 2/2016, all specified values are subject to change by SES-imagotag
www.ses-imagotag.com

B

Measurement Campaign - Channel Sounder

For the measurement campaign regular shelves were used. The shelves have a length of 1 m, a height of 2 m and a depth of 0.4 m. The shelves have 5 levels in total. The top level is referred to as level one while the level at the bottom is referred to as level five. Within the measurement campaign was the focus on the levels two to four since they are in a practically relevant height. At each level, ten positions were measured. The ten positions were equally spaced with a spacing of 10 cm. For each shelf the front side was defined as the side which points to the corridor. Each position on the shelf level was numbered. The first position was defined as the outermost position on the left side while the last position was the right outermost position. The first position was 5 cm to the right of the left side of the shelf. In Figure B.1 the 30 possible positions are illustrated for an ESL on a shelf.

Figure B.1: Positions of ESLs on a shelf

B.1 Standard Scenarios

The standard scenarios are defined as the scenarios where the transmitter ESLs were placed on shelves S7 and S8. For this scenario the transmitter ESL were placed on every possible position

on the shelves.

TX	ESL Nr.	Shelf	Shelf Level	Positions
1	8	7	1-3	1-10
2	9	8	1-3	1-10

Table B.1: Tx ESLs positions for the standard scenarios

While the transmitters were placed on various positions, the receiver ESLs within a scenario were always placed on the same positions. The position for the receiver ESLs can be found in the tables B.2 - B.6.

B.1.1 NLOS, facing

Rx	ESL Nr.	Shelf	Shelf Level	Position
1	1	2	4	3
2	2	2	4	8
3	3	2	3	4
4	4	2	3	10
5	5	1	3	5
6	6	1	2	3
7	7	1	2	8

Table B.2: Rx ESLs positions for NLOS, facing scenario

B.1.2 NLOS, aligned

Rx	ESL Nr.	Shelf	Shelf Level	Position
1	1	3	4	8
2	2	3	4	3
3	3	3	3	7
4	4	3	3	1
5	5	4	3	6
6	6	4	2	8
7	7	4	2	3

Table B.3: Rx ESLs positions for NLOS, aligned scenario

B.1.3 LOS 1

Rx	ESL Nr.	Shelf	Shelf Level	Position
1	1	6	4	3
2	2	6	4	8
3	3	5	4	3
4	4	5	4	8
5	5	5	3	9
6	6	5	3	6
7	7	5	3	2

Table B.4: Rx ESLs positions for LOS scenario, part 1

B.1.4 LOS 2

Rx	ESL Nr.	Shelf	Shelf Level	Position
1	1	6	2	3
2	2	6	2	8
3	3	5	2	3
4	4	5	2	8
5	5	6	3	9
6	6	6	3	5
7	7	6	3	2

Table B.5: Rx ESLs positions for LOS scenario, part 2

B.1.5 Rx Groups

Rx	ESL Nr.	Shelf	Shelf Level	Position
1	1	6	2	7
2	2	6	2	8
3	3	5	4	7
4	4	5	4	8
5	5	6	3	9
6	6	6	3	8
7	7	6	3	7

Table B.6: Rx ESLs positions for Rx group scenario

B.2 Special Scenarios

Special scenarios are characterized by the placement of the transmitter ESLs which is different than that from the definition in the standard scenario. The positions for the transmitter and receiver ESL are given in Table B.7 to B.11.

B.2.1 Same Shelf

Meas. Nr.	Tx	Shelf	Shelf Level	Position
1	1	6	2	2
	2	6	2	5
2	1	6	3	2
	2	6	2	6
3	1	6	3	3
	2	5	3	1
4	1	6	3	4
	2	5	3	2
5	1	6	3	6
	2	5	3	3
6	1	6	3	7
	2	5	3	4
7	1	6	3	8
	2	5	4	4
8	1	6	3	9
	2	5	4	5
9	1	5	3	9
	2	5	4	6
10	1	5	3	10
	2	5	4	7

Table B.7: Tx ESLs positions for same shelf scenario

Rx	ESL Nr.	Shelf	Shelf Level	Position
1	1	6	2	3
2	2	6	2	8
3	3	5	4	3
4	4	5	4	8
5	5	5	3	5
6	6	6	3	10
7	7	6	3	5

Table B.8: Rx ESLs positions for same shelf scenario

B.2.2 LOS, dense spacing

The transmitter ESLs were placed on the shelves S7 and S8 on the third level. Measurement were taken from positions which are equally spaced by 1 cm while the first and last positions are the same as for the other scenarios.

Rx	ESL Nr.	Shelf	Shelf Level	Position
1	1	6	2	3
2	2	6	2	8
3	3	5	4	3
4	4	5	4	8
5	5	5	3	5
6	6	6	3	10
7	7	6	3	5

Table B.9: Rx ESLs positions for dense LOS scenario

B.2.3 Groups on same shelf

Meas. Nr.	Tx	Shelf	Shelf Level	Position
1	1	6	2	2
	2	5	3	1
2	1	6	2	3
	2	5	3	2
3	1	6	2	4
	2	5	3	3
4	1	6	2	5
	2	5	3	4
5	1	6	2	6
	2	5	3	5
6	1	5	4	2
	2	5	3	6
7	1	5	4	3
	2	5	3	7
8	1	5	4	4
	2	5	3	8
9	1	5	4	5
	2	5	3	9
10	1	5	4	6
	2	5	3	10

Table B.10: Tx ESLs positions for groups on the same shelf scenario

Rx	ESL Nr.	Shelf	Shelf Level	Position
1	1	6	2	7
2	2	6	2	8
3	3	5	4	7
4	4	5	4	8
5	5	6	3	9
6	6	6	3	8
7	7	6	3	7

Table B.11: Rx ESLs positions for groups on the same shelf scenario

Tab. B.12 gives an overview of the used coax cables. The coax cables are labelled in order to distinguish them.

Device		Cable
Source	Destination	
Channel Sounder Tx	Switch 1.D - COM	Sukoflex 5
Channel Sounder Rx 1	Switch 1.A - COM	4_1
Channel Sounder Rx 2	Switch 2 COM	4_2
Switch 1.A - 1	Switch 1.B - COM	0.5_1
Switch 1.A - 2	Switch 1.C - COM	0.5_4
Switch 1.B - 1	ESL 1	2_1
Switch 1.B - 2	ESL 2	2_2
Switch 1.C - 1	ESL 3	2_3
Switch 1.C - 2	ESL 4	2_4
Switch 2.1	ESL 5	2_5
Switch 2.2	ESL 6	2_6
Switch 2.3	ESL 7	2_7
Switch 1.D - 1	ESL 8	12_1
Switch 1.D - 2	ESL 9	15_2

Table B.12: Used cables for the connection of the single devices

C

Measurement Campaign - Electronic Shelf Label

C.1 ESL Position

ESL ID	Shelf	Shelf Level	Position
B608E914	8	2	3
B6091FC5	8	2	8
B609A225	7	2	3
B61BA1DD	7	2	8
B61D02FE	8	3	3
B61D032D	8	3	8
B61D034E	7	3	3
B61D036D	7	3	8
B61D036F	6	2	3
B61D0372	6	2	8
B61D038E	5	2	3
B61D0393	5	2	8
B61D03CD	6	3	3
B61D03EE	6	3	8
B61D03F2	5	3	3
B61D040C	5	3	8
B61D0428	4	2	3
B61D044C	4	2	8
B61D0454	3	2	3
B61D0475	3	2	8
B61D04B2	4	3	3
B61D04B3	4	3	8
B61D04EB	3	3	3
B61D0619	3	3	8
B61D065A	2	2	3
B61D065D	2	2	8
B61D065F	1	2	3
B61D0679	1	2	8
B61D067D	2	3	3
B61D069D	2	3	8
B61D06BD	1	3	3
B61D06FD	1	3	8

C.2 RSSI Measurement

In Figure C.1 the overall setup of the RSSI measurement is illustrated. One ESL is defined as a Rx while all other ESLs are defined as Tx. All ESLs are controlled by a central instance which is an access point connected to a PC.

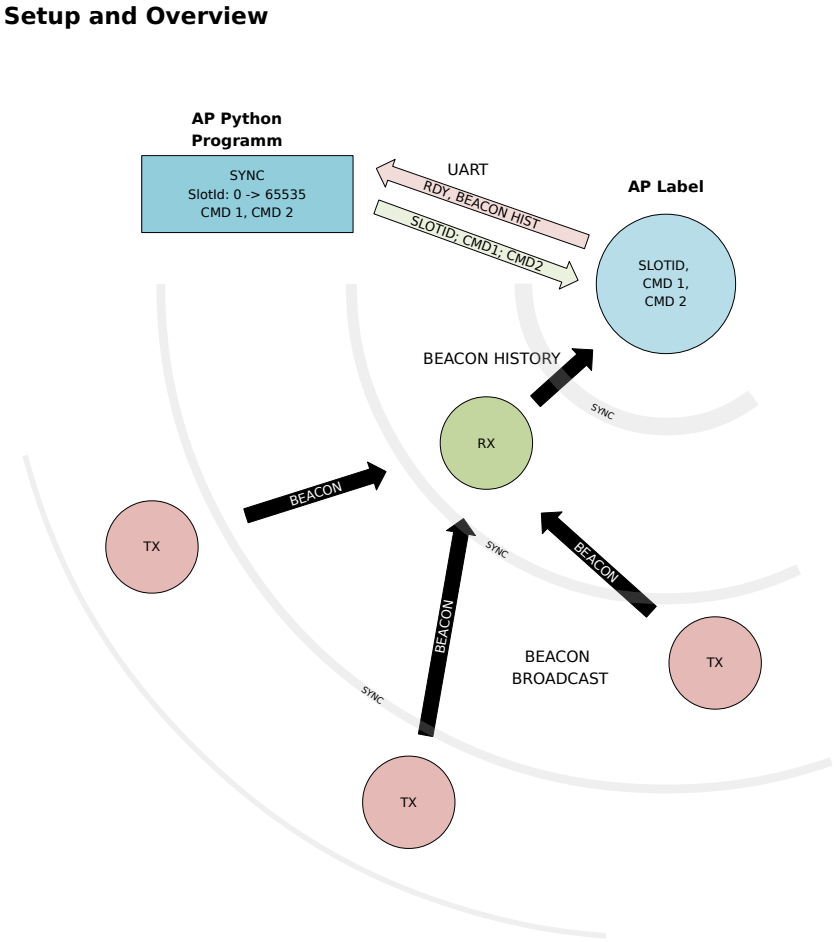

Figure C.1: Setup

Figure C.2 illustrates the synchronization procedure of the ESLs. The AP sends periodically synchronization frames which set the ESLs into Tx and Rx mode, see Figur C.3. The synchronization frame addresses a single ESL and defines its mode. First, an ESL is defined as an Rx which replies in return the history of received beacon frames and the corresponding RSSI values. Second, the remaining ESLs are set consecutively into Tx mode and broadcasts a beacon message which is received by the Rx Label. After all remaining ESLs were assigned ones as a Tx, the Rx ESL reports the beacon history to the AP. This procedure is repeated a predefined number. A detailed description of the single frames can be found in Figure C.3.

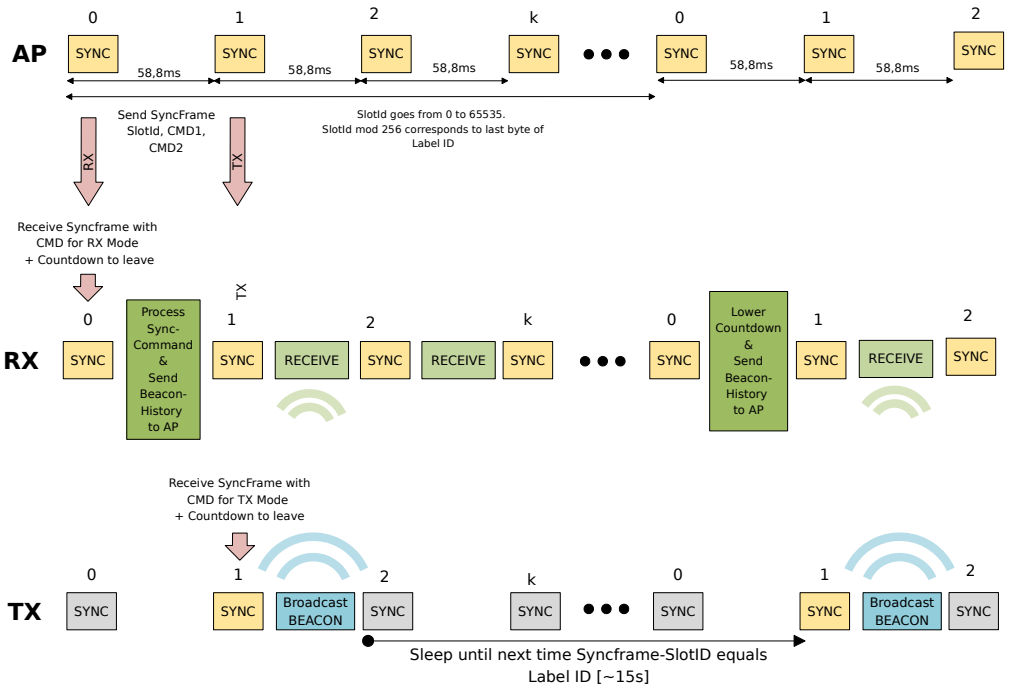

Figure C.2: Frame scheduling

SYNC frame definition:

Base Header 12 bytes [AP -> Label] Length: Dst: FF.FF.FF.FF Src: AP PORT: 0x3F DevInfo: 0x01 TractID	**Packet Type** 1 byte > SYNCFRAME > BEACON > PING > BEACONHIST REPLY	**Slot Id** 2 bytes	**CMD 1** 1 byte 0x00 – LOC Mode 0x01 – ESL Mode	**CMD 2** 1 byte 7 - 5 bit: Mode 4 - 3 bit: Base 2 - 0 bit: Mutiplicator

Packet Type corresponds to REPLY_TYPE enum in command.h
CMD 1 is reserved for change to ESL mode, Firmwareupdate etc.
CMD 2 defines Label Localization Mode and sets countdown.

0 Keep curr. Mode
1 TX Mode
2 RX Mode
3 Ping Mode
4 Delete and Sleep
5 free
6 free
7 free

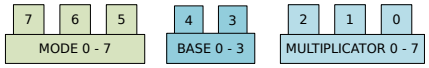

Base specifies numbers of sync frames to multiply with.
Example: base 3 (+1), multiplicator 5
(3+1) * 5 = 20 Syncs ≙ 300 seconds

BEACON / PING frame definition:

Base Header 12 bytes [AP -> Label] Length: Dst: FF.FF.FF.FF Src: AP PORT: 0x3F DevInfo: 0x01 TractID	**Packet Type** 1 byte > BEACON || PING	**Slot Id** 2 bytes

BEACON and PING frame are the same. Except for Packet Type. AP only listens to PING and ignores BEACONS.
BEACON FRAME is sent from TX Label every time SlotId is NOT LabelSlotId.
PING is queried by AccessPoint (gets RSSI and Labelstatus)

BEACON HIST REPLY frame definition:

Base Header 12 bytes [AP -> Label] Length: Dst: FF.FF.FF.FF Src: AP PORT: 0x3F DevInfo: 0x01 TractID	**Packet Type** 1 byte > BEACONHIST REPLY	**BEACONHIST[4]** 28 bytes BEACONHIST: SRC ADDRESS Last RSSI Beacon SlotId

When Label is in RX Mode it Replies with multiple BEACONHIST_REPLY packets each containing an array of BEACONHIST.
Maximum number of BEACONHIST_REPLY packets = 4, each containing 4 unique Beacon Frames from one TX Label

Figure C.3: Definition of the frames

Bibliography

[1] K. Witrisal, P. Meissner, E. Leitinger, Y. Shen, C. Gustafson, F. Tufvesson, K. Haneda, D. Dardari, A. F. Molisch, A. Conti, and M. Z. Win, "High-accuracy localization for assisted living - 5g systems will turn multipath channels from foe to friend," *IEEE Signal Processing Magazine*, 2016, special Issue on Assisted Living.

[2] "Application scenario of electronic shelf labels," online, Apr. 2018. [Online]. Available: https://www.ses-imagotag.com/en/references/

[3] H. Liu, H. Darabi, P. Banerjee, and J. Liu, "Survey of wireless indoor positioning techniques and systems," *IEEE Transactions on Systems, Man, and Cybernetics, Part C (Applications and Reviews)*, vol. 37, no. 6, pp. 1067–1080, Nov 2007.

[4] R. Zekavat and R. Buehrer, *Handbook of Position Location: Theory, Practice and Advances*, ser. IEEE Series on Digital & Mobile Communication. Wiley, 2011. [Online]. Available: https://books.google.at/books?id=2kJuNmtDMkgC

[5] P. Meissner, "Multipath-assisted indoor positioning," phdthesis, Graz University of Technology, Oct. 2014. [Online]. Available: https://www.spsc.tugraz.at/sites/default/files/MeissnerPhDThesis2014web_0.pdf

[6] A. Popleteev, "Indoor localization using ambient fm radio rss fingerprinting: A 9-month study," in *2017 IEEE International Conference on Computer and Information Technology (CIT)*, Aug 2017, pp. 128–134.

[7] A. Schwaighofer, M. Grigoraş, V. Tresp, and C. Hoffmann, "Gpps: A gaussian process positioning system for cellular networks," in *Advances in Neural Information Processing Systems 16*. MIT Press, January 2004, p. 579–586. [Online]. Available: https://www.microsoft.com/en-us/research/publication/gpps-a-gaussian-process-positioning-system-for-cellular-networks/

[8] S. Mazuelas, A. Bahillo, R. M. Lorenzo, P. Fernandez, F. A. Lago, E. Garcia, J. Blas, and E. J. Abril, "Robust indoor positioning provided by real-time rssi values in unmodified wlan networks," *IEEE Journal of Selected Topics in Signal Processing*, vol. 3, no. 5, pp. 821–831, Oct 2009.

[9] N. Salman, M. Ghogho, and A. H. Kemp, "On the joint estimation of the rss-based location and path-loss exponent," *IEEE Wireless Communications Letters*, vol. 1, no. 1, pp. 34–37, February 2012.

[10] A. Golestani, N. Petreska, D. Wilfert, and C. Zimmer, "Improving the precision of rssi-based low-energy localization using path loss exponent estimation," in *2014 11th Workshop on Positioning, Navigation and Communication (WPNC)*, March 2014, pp. 1–6.

[11] J. Talvitie, "Algorithms and methods for received signal strength based wireless localization," Ph.D. dissertation, 1 2016, awarding institution:Tampere University of Technology.

[12] V. Honkavirta, T. Perala, S. Ali-Loytty, and R. Piche, "A comparative survey of wlan location fingerprinting methods," in *2009 6th Workshop on Positioning, Navigation and Communication*, March 2009, pp. 243–251.

[13] M. Schüssel and F. Pregizer, "Coverage gaps in fingerprinting based indoor positioning: The use of hybrid gaussian processes," in *2015 International Conference on Indoor Positioning and Indoor Navigation (IPIN)*, Oct 2015, pp. 1–9.

[14] P. Bahl, V. N. Padmanabhan, V. Bahl, and V. Padmanabhan, "Radar: An in-building rf-based user location and tracking system." Institute of Electrical and Electronics Engineers, Inc., March 2000. [Online]. Available: https://www.microsoft.com/en-us/research/publication/radar-an-in-building-rf-based-user-location-and-tracking-system/

[15] M. 36, "Verkaufsstätten - richtlinie der magistratsabteilung 36," Dresdner Straße 73 - 75 1200 Wien, 03 2016. [Online]. Available: https://www.wien.gv.at/wirtschaft/gewerbe/technik/pdf/verkaufsstaettenrichtlinie.pdf

[16] A. F. Molisch, *Wireless communications*, 2nd ed. Weinheim: Wiley [u.a.], 2011;2010;.

[17] P. Pagani, F. T. Talom, P. Pajusco, and B. Uguen, *UWB Propagation Channel Sounding*. ISTE, 2010, pp. 67–98. [Online]. Available: http://dx.doi.org/10.1002/9780470611715.ch3

[18] M. Lafer, "Real-time multipath-assisted indoor tracking and feature detection," Master's thesis, Graz University of Technology, February 2014.

[19] C. A. Balanis, *Antenna theory: analysis and design*, 4th ed., 2016.

[20] H. Arthaber, J. Soklic, and D. Neunteufel, "Ses-imagotag rssi measurements," Institute of Electrodynamics, Microwave and Circuit Engineering TU Wien, Gußhausstraße 25/354 1040 Vienna Austria, techreport 2.1, Feb. 2018.

[21] T. S. Rappaport, *Wireless communications: principles and practice*, 2nd ed. Upper Saddle River, NJ: Prentice Hall PTR, 2002.

[22] J. G. Proakis, *Digital communications*, 3rd ed. New York, NY [u.a.]: McGraw-Hill, 1995.

[23] G. Stüber, *Principles of Mobile Communication*. Springer New York, 2014. [Online]. Available: https://books.google.at/books?id=-LQFogEACAAJ

[24] K. Witrisal, "Ofdm air-interface design for multimedia communications," Ph.D. Thesis, Delft Univ. of Technology, 2002.

[25] T. Pedersen, "Contributions in radio channel sounding, modeling, and estimation," Ph.D. dissertation, 2009.

[26] A. A. M. Saleh and R. Valenzuela, "A statistical model for indoor multipath propagation," *IEEE Journal on Selected Areas in Communications*, vol. 5, no. 2, pp. 128–137, February 1987.

[27] J. B. Andersen, J. O. Nielsen, G. F. Pedersen, G. Bauch, and J. M. Herdin, "Room electromagnetics," *IEEE Antennas and Propagation Magazine*, vol. 49, no. 2, pp. 27–33, April 2007.

[28] J. B. Andersen, J. O. Nielsen, G. Bauch, and M. Herdin, "The large office environment - measurement and modeling of the wideband radio channel," in *2006 IEEE 17th International Symposium on Personal, Indoor and Mobile Radio Communications*, Sept 2006, pp. 1–5.

[29] G. Steinböck, T. Pedersen, B. H. Fleury, W. Wang, and R. Raulefs, "Experimental validation of the reverberation effect in room electromagnetics," *IEEE Transactions on Antennas and Propagation*, vol. 63, no. 5, pp. 2041–2053, May 2015.

[30] G. Steinböck, T. Pedersen, B. H. Fleury, W. Wang, and R. Raulefs, "Distance dependent model for the delay power spectrum of in-room radio channels," *IEEE Transactions on Antennas and Propagation*, vol. 61, no. 8, pp. 4327–4340, Aug 2013.

[31] G. Steinbock, T. Pedersen, B. H. Fleury, W. Wang, T. Jost, and R. Raulefs, "Model for the path loss of in-room reverberant channels," in *2011 IEEE 73rd Vehicular Technology Conference (VTC Spring)*, May 2011, pp. 1–5.

[32] D. Arnitz, "Tag localization in passive uhf rfid," phdthesis, Graz University of Technology, May 2011.

[33] H. Wymeersch, J. Lien, and M. Z. Win, "Cooperative localization in wireless networks," *Proceedings of the IEEE*, vol. 97, no. 2, pp. 427–450, Feb 2009.

[34] A. T. Ihler, J. W. Fisher, R. L. Moses, and A. S. Willsky, "Nonparametric belief propagation for self-localization of sensor networks," *IEEE Journal on Selected Areas in Communications*, vol. 23, no. 4, pp. 809–819, April 2005.